ISTANBUL TECHNICAL UNIVERSITY ★ GRADUATE SCHOOL

CREEP BEHAVIOR INVESTIGATION OF 3D PRINTED POLYETHERIMIDE PARTS WITH CARBON BLACK REINFORCEMENT VIA EXPERIMENTAL ANALYSIS AND MODELING

M.Sc. THESIS

Merve KARABAL

Department of Aeronautical and Astronautical Engineering

Aeronautical and Astronautical Engineering Programme

JULY 2024

ISTANBUL TECHNICAL UNIVERSITY ★ GRADUATE SCHOOL

CREEP BEHAVIOR INVESTIGATION OF 3D PRINTED POLYETHERIMIDE PARTS WITH CARBON BLACK REINFORCEMENT VIA EXPERIMENTAL ANALYSIS AND MODELING

M.Sc. THESIS

Merve KARABAL
(511221123)

Department of Aeronautical and Astronautical Engineering

Aeronautical and Astronautical Engineering Programme

Thesis Advisor: Asst. Prof. Alptekin YILDIZ

JULY 2024

İSTANBUL TEKNİK ÜNİVERSİTESİ ★ LİSANSÜSTÜ EĞİTİM ENSTİTÜSÜ

3B BASILMIŞ KARBON SİYAHI TAKVİYELİ POLİETERİMİD PARÇALARIN DENEYSEL ANALİZ VE MODELLEME İLE SÜRÜNME DAVRANIŞININ İNCELENMESİ

YÜKSEK LİSANS TEZİ

Merve KARABAL
(511221123)

Uçak ve Uzay Mühendisliği Anabilim Dalı

Uçak ve Uzay Mühendisliği Programı

Tez Danışmanı: Asst. Prof. Alptekin YILDIZ

TEMMUZ 2024

Merve KARABAL, a M.Sc. student of ITU Graduate School student ID 511221123 successfully defended the thesis entitled "CREEP BEHAVIOR INVESTIGATION OF 3D PRINTED POLYETHERIMIDE PARTS WITH CARBON BLACK REINFORCEMENT VIA EXPERIMENTAL ANALYSIS AND MODELING", which she prepared after fulfilling the requirements specified in the associated legislations, before the jury whose signatures are below.

Thesis Advisor : **Asst. Prof. Alptekin YILDIZ** ....
Istanbul Technical University

Jury Members : **Prof. Dr. Hülya CEBECİ** ....
Istanbul Technical University

Asst. Prof. Fatih USTA ....
Gebze Technical University

....

Date of Submission : **4 July 2024**
Date of Defense : **26 July 2024**

To my family,

FOREWORD

First and foremost, I would like to express my deepest gratitude to my advisor, Asst. Prof. Alptekin YILDIZ, for his invaluable guidance, support, and insightful advice throughout my entire master's education. His constructive criticisms have been instrumental in shaping the quality of this thesis and pushing me to achieve my best.

I am also profoundly thankful to Prof. Dr. Hülya CEBECİ for her encouragement and mentorship throughout my master's program.

Special thanks to my colleague Ramazan YÜKSEL for his cooperation and all his assistance with the experiments. I would also like to extend my sincere thanks to my colleagues in the Nanomaterials, Textiles, and Advanced Composites Research Group at the Aerospace Research Center, Istanbul Technical University, for their valuable discussions.

Finally, I am extremely grateful to my family for their unwavering support and encouragement. Their belief in me has been a constant source of motivation. I also want to thank my friends for their continuous motivation and for being with me throughout the thesis process.

July 2024

Merve KARABAL
(Aeronautical Engineer)

TABLE OF CONTENTS

ABBREVIATIONS

3D	: 3-Dimensional
ABS	: Acrylonitrile butadiene styrene
Adj.	: Adjusted
AM	: Additive Manufacturing
CB	: Carbon Black
CF	: Carbon Fiber
CNT	: Carbon Nanotube
D	: Diameter
DMA	: Dynamical Mechanical Analysis
DTG	: Derivative Thermogravimetric
FFF	: Fused Filament Fabrication
GNP	: Graphene Nanoplatelet
HDPE	: High-density polyethylene
L	: Length
PEI	: Polyetherimide PEI
PEEK	: Polyether ether ketone
PLA	: Polylactic acid
PPS	: Polyphenylene Sulfide
PPSU	: Polyphenylsulfone
PVC	: Polyvinyl chloride
Red.	: Reduced
SCF	: Short Carbon Fiber
SEM	: Scanning Electron Microscopy
TGA	: Thermogravimetric Analysis
TTSP	: Time-Temperature Superposition Principle
UTM	: Universal Testing Machine
UTS	: Ultimate Tensile Strength
WLF	: William-Landel-Ferry

SYMBOLS

a_T	: Shift factor
E	: Stiffness
E_a	: Activation Energy
η	: Viscosity
σ_0	: Constant stress
σ_e, σ_v	: Elastic and viscous applied stress
$\dot{\sigma}$	: Stress rate
ε_e, ε_v	: Elastic and viscous strain
$\dot{\varepsilon}_e$, $\dot{\varepsilon}_v$	: Elastic and viscous strain rate
T_g	: Glass transition temperature
T_{max}	: Maximum thermal degradation temperature
T_{onset}	: Onset thermal degradation temperature
T_{ref}	: Reference temperature
kN	: kilo Newton
min.	: minutes
mm	: milimeter
nm	: nanometer
Pa	: Pascal
rad	: Radian
R	: Universal gas constant
S	: Siemens
μ**m**	: micrometer
MPa	: Mega Pascal
wt%	: weight%

LIST OF TABLES

LIST OF FIGURES

CREEP BEHAVIOR INVESTIGATION OF 3D PRINTED POLYETHERIMIDE PARTS WITH CARBON BLACK REINFORCEMENT VIA EXPERIMENTAL ANALYSIS AND MODELING

SUMMARY

Additive manufacturing (AM) technologies, also known as 3D printing technologies, have garnered significant attention across various sectors due to their distinct production methodology compared to conventional manufacturing methods. AM technologies based on a principle of building geometries layer by layer, offering advantages such as minimum waste material, the ability to produce complex geometries in a single process, no need for assembly, and the elimination of initial investment costs. Initially introduced for rapid prototyping, AM has evolved with technological advancements, leading to more precise product dimensions, faster part production, and a broader range of raw materials. Consequently, it has found applications in aerospace, automotive, and medical sectors.

Fused Filament Fabrication (FFF) technology is the most widely used AM technology for polymeric part production. Its popularity stems from nearly zero waste production, accessibility and ease of use of FFF printers, and relatively low production costs compared to other AM technologies. Despite its many advantages, FFF-produced parts often exhibit lower mechanical performance compared to their conventionally manufactured counterparts, and the relatively slow production speeds limit their use in high-strength demanding fields.

In recent years, researchers have focused on using high-performance thermoplastics in FFF applications to overcome these limitations. High-performance thermoplastics, such as polyetherimide (PEI), maintain their mechanical strength at high temperatures and exhibit greater chemical and thermal stability compared to commonly used thermoplastics like polylactic acid (PLA) and acrylonitrile butadiene styrene (ABS). PEI filaments, with a high glass transition temperature (T_g), high tensile strength, and thermal stability, are suitable for use as load-bearing functional components. Additionally, PEI's flame retardancy, low smoke density, and low toxicity make it an ideal material for aerospace applications. Its low coefficient of thermal expansion and amorphous structure further enhance its dimensional stability, making it suitable for FFF.

The corporation of various reinforcement materials to PEI filaments to create composite materials has been shown to enhance the performance of FFF-produced parts for advanced technological applications. Carbon-based reinforcements like carbon nanotubes (CNT), graphene, carbon black (CB), and carbon fiber (CF) improve the mechanical properties of neat thermoplastic filaments and impart additional features such as electrical and thermal conductivity, making them multifunctional.

These developments have increased the importance of composite materials in high-performance applications and brought new opportunities for their employment.

This thesis investigated the potential of overcoming the mechanical weaknesses of FFF-produced parts compared to their conventionally manufactured counterparts by reinforcing PEI with CB particles. The study systematically investigates the recovery of mechanical strength lost due to the layered structure inherent in AM by adding varying amounts of CB. Samples were characterized using various techniques, with a focus on their creep behavior, and compared to conventionally produced samples. Additionally, the creep behavior of the samples was further analyzed through mathematical modeling.

First of all, composite filaments consisting of neat PEI and varying concentrations of CB (5%, 10%, and 20% by weight (wt)) were prepared using a co-rotating twin-screw extruder. Creep test samples were produced from these filaments using a 3D printer specifically designed for printing high-performance thermoplastics. To compare the mechanical properties of FFF-produced samples with those produced conventionally, neat PEI creep test samples were also manufactured using the hot-press technique.

The thermal, rheological, morphological, and mechanical characterizations of the composite filaments were conducted to evaluate the CB reinforcement effects. Thermogravimetric analysis (TGA) revealed that PEI experienced no significant weight loss up to 500 °C. The initial thermal degradation temperatures of all samples were calculated, showing that CB did not significantly affect this temperature. Rheological measurements indicated that the storage moduli and complex viscosities of all filaments increased with CB content, reaching a rheological percolation threshold around 10 wt% CB. Scanning electron microscope (SEM) analysis confirmed adequate dispersion of CB within the PEI matrix. Tensile tests showed that 5 wt% CB reinforcement resulted in the highest tensile strength, with strength decreasing slightly at 10 wt% and reducing significantly at 20 wt% due to brittleness.

Creep tests conducted between 30 °C and 190 °C, in 20 °C increments, with a 3 MPa load applied for 10 minutes, demonstrated that increasing CB content improved the creep resistance of the composites. The 5 wt% CB/PEI samples exhibited the least creep deformation and similar behavior to conventionally produced neat PEI samples, indicating that the mechanical strength lost in FFF-produced samples could be recovered with CB reinforcement. Finally, experimental creep data were simulated using viscoelastic models. The Burgers and Findley power law models successfully modeled the behavior, with the Findley power law showing better alignment with experimental results. The generalized Kelvin-Voigt model, despite fitting the curves well, provided inconsistent parameter values. The study concluded with the creation of time-temperature superposition principle (TTSP) master curves, where manual shifting using Python provided the most reasonable results.

This thesis aims to enhance the mechanical properties of high-performance composite materials produced via FFF, thereby increasing their potential use in advanced technological applications. The findings contribute significantly to the broader industrial application of FFF-based 3D printers by optimizing the mechanical strength and creep resistance of PEI and CB-reinforced composites.

3B BASILMIŞ KARBON SİYAHI TAKVİYELİ POLİETERİMİD PARÇALARIN DENEYSEL ANALİZ VE MODELLEME İLE SÜRÜNME DAVRANIŞININ İNCELENMESİ

ÖZET

Eklemeli imalat (Eİ) teknolojileri, diğer adıyla 3B yazıcı teknolojileri, konvansiyonel üretim yöntemlerine kıyasla farklı bir üretim metodolojisi benimseyerek getirdiği yenilikçi bakış açısıyla çeşitli sektörlerde dikkat çekmiş ve hızla yaygınlaşmıştır. Prensip olarak üretilecek geometrileri katmanlar halinde üst üste ekleyerek inşa etmeye dayanan Eİ metodolojisi, karmaşık geometrilere sahip parçaların tek seferde üretilmesini sağlar ve montajlama ihtiyacını ortadan kaldırır. Ayrıca, az miktarda atık hammadde oluşturması ve kalıplama maliyeti gibi başlangıç yatırımları gerektirmemesi gibi avantajları ile konvansiyonel üretim yöntemlerinin bir adım önüne çıkar. İlk olarak hızlı prototipleme amacıyla piyasaya sürülen Eİ, teknolojinin de gelişmesiyle birlikte daha hassas ürün boyutlandırma, hızlı parça üretimi ve hammaddedeki çeşitlilikle birlikte hızla farklı sektörelere yayılmış, havacılık-uzay, otomotiv ve medikal gibi sektörlerde de tercih edilmeye başlanmıştır. Eriyik Yığma Modelleme (EYM) teknolojisi, diğer eklemeli imalat teknolojileri arasında polimerik parça üretiminde en çok tercih edilen Eİ teknolojisidir. Bunun başlıca sebepleri, üretim esnasında neredeyse sıfır atık çıkması, EYM yazıcılarının ulaşılabilir ve kullanımının kolay olması ve diğer Eİ teknolojilerine nispeten düşük maliyetli bir üretim yöntemi olmasıdır. EYM'nin birçok avantaja sahip olmasına rağmen, elde edilen ürünlerin mekanik performansının konvansiyonel üretim yöntemleriyle üretilen muadillerine göre düşük olması ve görece yavaş üretim hızları nedeniyle yüksek dayanım isterleri olan havacılık ve uzay teknolojileri alanında kullanımları sınırlıdır.

Ancak, araştırmacılar son yıllarda yüksek performanslı termoplastiklerin EYM yöntemi ile parça üretiminde kullanılması üzerine çalışmalarını sürdürmektedirler. Bu da ileri teknoloji alanında bu parçaların kullanımının önünü açmaktadır. Yüksek performanslı termoplastikler, poli laktikasit (PLA) ve akrilonitril bütadien stiren (ABS) gibi yaygın kullanılan termoplastiklere kıyasla yüksek sıcaklıklarda mekanik dayanımlarını koruyabilirler. Ayrıca, moleküler yapıları sayesinde kimyasal ve termal olarak daha kararlıdırlar. Polieterimid (PEI) filamanlar, yüksek performanslı termoplastikler arasında EYM uygulamalarında en çok tercih edilen termoplastiklerden biridir. Yüksek camsı geçiş sıcaklığı (217 °C), yüksek çekme dayanımı ve termal kararlılığı ile yük taşıyıcı fonksiyonel elemanlar olarak kullanıma elverişlidir. Ayrıca, alev geciktirici özelliği, düşük duman yoğunluğu ve düşük toksisite göstermesi PEI'yi havacılık uygulamaları için ideal bir malzeme yapar. Ek olarak, düşük genleşme katsayısı ve amorf yapısı PEI'nin boyutsal stabilitesini artıran dolayısıyla da EYM için elverişli kılan diğer önemli faktörlerdendir. PEI filamanlara eklenen çeşitli takviye malzemeleri ile oluşturulan kompozit malzemelerin EYM ile üretilmiş parçaların

ileri teknoloji uygulamalarında kullanımını artırdığı görülmüştür. Özellikle karbon nanotüp (KNT), grafen, karbon siyahı (KS) ve karbon fiber (KF) gibi karbon temelli takviye malzemeleri, saf termoplastik filamanların mekanik özelliklerini geliştirmekte ve ayrıca elektriksel iletkenlik, termal iletkenlik gibi özellikler kazandırarak çok fonksiyonlu hale getirmektedir. Bu gelişmeler, yüksek performans gerektiren alanlarda kullanılan kompozit malzemelerin önemini artırmakta ve yeni uygulama alanları açmaktadır.

Bu tez çalışmasında, eklemeli imalatın doğası gereği katmanlı yapıda üretimin neden olduğu, konvansiyonel üretim yöntemi ile üretilen muadillerine kıyasla görülen düşük mekanik özelliklerin telafi edilmesi amaç edinilmiştir. karbon bazlı muadillerine kıyasla oldukça düşük maaliyetli KS takviyesi yapılarak PEI'nin mekanik özellikleri iyileştirilmeye ve konvansiyonel üretim seviyesine çıkarılmaya çalışılmıştır. Farklı miktarlarda KS takviye edilerek eklemeli imalat nedeniyle kaybedilen mekanik dayanımın geri kazanımı sistematik olarak incelenmiştir. Bu amaçla, çeşitli karakterizasyon yöntemleriyle numuneler karakterize edilmiş, özellikle numunelerin sürünme davranışı incelenmiş ve konvansiyonel yöntemlerle üretilmiş numuneler ile karşılaştırılmıştır. Ayrıca, numunelerin sürünme davranışı deneysel karakterizasyonlara ek olarak matematiksel modellemelerle daha iyi anlaşılmaya ve tahmin edilmeye çalışılmıştır.

Çalışmaya kompozit filamanların üretimi ve numunelerin hazırlanması ile başlanmıştır. Saf PEI ve farklı oranlarda KS (ağırlıkça (ağ.) %5, %10 ve %20) içeren kompozit 3B yazıcı filamanları, eş dönüşlü çift vidalı ekstrüder kullanılarak hazırlanmıştır. Elde edilen bu filamanlardan, yüksek performanslı polimerler için özel olarak tasarlanmış bir 3B yazıcı kullanılarak, sürünme testi numuneleri üretilmiştir. Ayrıca, KS takviyesinin kazandırdığı mekanik özellikleri konvansiyonel üretimle karşılaştırmak amacıyla, sıcak presleme yöntemi kullanılarak saf PEI sürünme testi numunesi de üretilmiştir.

İlk olarak, elde edilen kompozit filamanların, KS takviyesi ile değişen termal, reolojik, morfolojik ve mekanik karakterizasyonları gerçekleştirilerek KS eklenmesinin etkileri anlaşılmaya çalışılmıştır. Saf PEI, ağ. %5, %10 ve %20 KS/PEI filamanlarından granül numuneler kırpılarak termogravimetrik analiz yapılmıştır. Analiz sonucunda PEI'nin 500 °C'ye kadar kayda değer bir kütle kaybı yaşamadığı gözlemlenmiştir. Ek olarak, tüm numunelerin başlangıç termal bozunma sıcaklıkları hesaplanmış ve KS'nin bu sıcaklığı önemli ölçüde etkilemediği görülmüştür. Benzer şekilde, granül formuna getirilen tüm KS konsantrasyonlarındaki filamanların reometre cihazı kullanılarak depolama modülleri ve kompleks viskoziteleri ölçülmüştür. Ağ. %5 KS takviye miktarı aşıldıktan sonra mikro yapının değişmeye başladığı ve %10 KS civarında reolojik sızma eşiğine ulaşıldığı görülmektedir. Ayrıca KS ile birlikte kompleks viskozitenin aniden arttığı ancak PEI'nin artan frekansa bağlı olarak kayma incelmesi (shear thinning) davranışı gösterdiği gözlemlenmiştir. KS'nin PEI matrisi içerisinde homojen dağılıp dağılmadığını incelemek ve kompozitlerin üretim kalitesi hakkında yorum yapmak amacıyla taramalı elektron mikroskobunda filaman kesitleri incelenmiştir. PEI matris içerisinde KS'nin küçük agregalar halinde yeterli bir şekilde dağıldığı görülmüştür. Son olarak, KS katkısının filamanların çekme dayanımlarına olan etkisini araştırmak için evrensel çekme cihazı kullanılarak maksimum çekme dayanımları incelenmiştir. %5 KS oranında filamanlar en yüksek çekme dayanımı sonucunu vermiştir. Ağ. %10 KS miktarına ulaşıldığında çekme dayanımı hafifçe düşmüş ve Ağ. %20'de aşırı KS yüklemesiyle son derece kırılgan yapıya sahip olan filamanların çekme dayanımları aniden düşmüştür.

Filaman karakterizasyonu tamamlandıktan sonra KS katkısının eklemeli imalatla üretilen numunelerin mekanik performansını konvansiyonel numunelerle karşılaştırmak için sürünme testleri yürütülmüştür. 30 °C - 190 °C aralığında, 20 °C aralıklarla, 3B basılmış saf PEI, Ağ. %5 ve %10 katkılı numunelere ve sıcak preslenmiş saf PEI numuneye 10 dakika boyunca 3 MPa yük uygulanmış ve sürünme gerinimleri ölçülmüştür. Ağ. %20 katkılı filamanların son derece kırılgan yapısından dolayı efektif baskılar alınamadığı için sürünme testlerine dahil edilmemiştir. Yapılan sürünme testleri sonucunda, KS içeriğinin artmasıyla kompozitlerin sürünme direncinin arttığı, sürünme deformasyonlarının azaldığı ve yüksek sıcaklıklarda bu etkinin daha belirgin hale geldiği belirlenmiştir. Özellikle %5 KS/PEI numunelerinin sürünme deformasyonunun en az olduğu ve konvansiyonel yöntemle üretilen saf PEI numuneleriyle benzer davranışlar sergilediği görülmüştür. Böylelikle eklemeli imalat ile kaybedilen dayanım değerleri KS takviyesi ile tekrar kazanılabilmiştir.

Son olarak, deneysel sürünme verileri, viskoelastik fonksiyonlar kullanılarak simüle edilmiştir. Burgers, Findley güç yasası ve genelleştirilmiş Kelvin-Voigt modelleri kullanılarak detaylı bir şekilde incelenmiştir. Burgers ve Findley modelleri davranışları başarılı bir şekilde modellemiş, ancak Burgers modelinin elastik anlık gerinimi yakalamakta zorlandığı, buna karşılık Findley güç yasasının deneysel sonuçlarla daha uyumlu eğriler oluşturduğu tespit edilmiştir. Genelleştirilmiş Kelvin-Voigt modelinde ise eğri uydurma sonuçları deneysel sonuçlarla çok uyumlu görünse de parametre değerleri tutarlı sonuçlar vermemiştir. Çalışma, tüm numunelere ait zaman-sıcaklık süperpozisyon (TTS) eğrilerinin oluşturulmasıyla sonlandırılmıştır. Sürünme eğrilerinin kaydırılarak bir ana eğri elde edilmesi için gerekli kaydırma faktörleri dört farklı yöntem kullanılarak elde edilmeye çalışılmıştır. Arrhenius ve William-Landel-Ferry (WLF) yöntemleri PEI'nin termo-mekanik olarak karmaşık yapıya sahip bir polimer olması nedeniyle başarılı olamamıştır. Literatürde yeni bir yöntem olan MNAT prosedürü kullanılarak makul bir sürünme ana eğrisi elde edilmiştir, ancak sürünme ana eğrisi zaman ekseninde 10^{18} saniyelere kadar uzamıştır, bu da gerçekçi sonuçlar vermemiştir. Son olarak, Python kullanılarak deneysel verileri manuel kaydıracak bir kod yazılmış ve TTS ana eğrisi elde edilmiştir.

Bu tez, EYM yöntemiyle üretilen yüksek performanslı kompozit malzemelerin mekanik özelliklerini düşük maaliyetli ama etkili bir yöntemle geliştirerek, ileri teknoloji uygulamalarında kullanım potansiyelini artırmayı amaçlamıştır. Bu bağlamda, PEI ve KS takviyeli kompozitlerin mekanik dayanımını ve sürünme direncini optimize etmek için yapılan çalışmalar, EYM temelli 3B yazıcıların endüstriyel uygulamalarda daha yaygın olarak kullanılmasının önünü açmaktadır.

1. INTRODUCTION

1.1 Purpose of Thesis

AM has been gaining popularity in the last few decades with its advantages, such as the ability to produce intricate geometries that are difficult to produce with conventional manufacturing methods, less waste material, and rapid prototyping. Among the several AM methods, FFF has gained attention not only in the industrial area but also within academic communities. The widespread adoption of FFF printers can be attributed to the ease of accessibility and the relatively low initial investment required compared to other manufacturing techniques like injection molding. Although FFF originated in its early days for the rapid and cost-effective production of prototypes, it has recently employed as a novel application providing design flexibility and a wide range of feedstock materials.

Despite significant benefits, 3D-printed parts still face considerable challenges related to lower mechanical properties, which hinder their employment as structural and functional components. The lower mechanical properties of FFF parts compared to injection molded counterparts significantly limit their use as functional and load-bearing elements in advanced engineering applications, highlighting the pressing need for solutions to enhance their performance. Recent research indicates a growing trend in employing FFF parts in advanced technological applications, driven by the availability of high-performance thermoplastics and their composites formulated with reinforcing fillers.

The primary objective of this thesis is to address the inherently lower mechanical properties of parts fabricated through FFF. By enhancing the mechanical characteristics of thermoplastic 3D-printer filaments through reinforcement strategy, the aim is to elevate their performance to a level competitive with, and potentially surpassing, that of conventionally manufactured parts. This enhancement aims to be achieved in a cost-effective yet highly efficient manner, breaking down barriers that currently inhibit the widespread adoption of the FFF method in demanding areas such as aerospace and defense industries.

To realize this objective, a comprehensive research methodology was followed. High-performance thermoplastic PEI, suitable for advanced engineering applications, was selected as the matrix material. This thermoplastic was reinforced with varying concentrations of CB, a cost-effective reinforcing material compared to other carbon-based alternatives, to produce composite 3D-printer filaments. The mechanical, thermal, morphological, and rheological performance of these composite filaments was investigated through a series of experimental analyses. Moreover, the creep behavior of test specimens printed using these composite filaments was examined and compared with a reference specimen of neat PEI produced via injection molding. This facilitated a comparative mechanical performance evaluation of FFF parts against conventionally manufactured components.

Beyond the experimental investigations, this thesis emphasizes the importance of mathematical modeling in understanding the creep properties of polymeric composites. By modeling the creep behavior based on experimental data, the thesis aims to provide an engineering perspective that allows for the prediction of the material's potential behavior. This dual approach of experimental analysis and mathematical modeling not only enhances the understanding of the creep characteristics of polymeric composites but also enables more precise predictions regarding their performance, thereby optimizing the design process.

1.2 Literature Review

FFF has gained attention among the several AM methods since it offers tailorable solutions with a wide range of feedstock materials and design flexibility. However, FFF parts still struggle with drawbacks associated with inferior mechanical properties, impeding their suitability in high-strength applications. The presence of porous structures and interlayer voids resulting from inadequate layer bonding diminishes the mechanical integrity of these parts [2,3]. Lay et al. [4] conducted a comperehensive study to compare the mechanical performance of PLA, ABS, and nylon 6 produced via injection molding and FFF. They measured the ultimate tensile strength (UTS), elastic modulus, and elongation at break and found that all properties in 3D-printed form decreased due to weak layer adhesion and gaps between layers. Similarly, Ding et al. [5] investigated the mechanical behaviors of FFF-printed PEI and Polyether ether ketone (PEEK) via different nozzle temperatures to compare with injection molding of ones. The results demonstrated that the tensile strength of printed PEI and PEEK was roughly 80% of the injection-molded ones. Since the injection molding technique provides high pressure, it increases the entanglement in the polymer chain, and thus, higher stiffness is obtained. High-performance thermoplastics, such as PEI and PEEK, are characterized by their ability to maintain mechanical integrity at elevated temperatures and exhibit thermal and chemical stability. As a result, these materials have paved the way for the potential use of FFF in advanced engineering applications [6]–[8]. Furthermore, researchers have explored reinforcing these thermoplastic polymers with various filler materials at nano- and micro-scales to offset potential reductions in mechanical properties. Commonly utilized carbon-based materials for reinforcing high-performance thermoplastics include CNT, CB, graphene nanoplatelets (GNP), CF [9,10]. For instance, Kaynan et al. [6] produced PEI filaments reinforced with CNT at various (2, 5, and 7 wt%)concentrations. These filaments exhibited a significant 55% increase in tensile modulus with a 5 wt% CNT fraction. Among carbon-based filler materials, CB stands out for its cost-effectiveness and versatility in reinforcing elastomers and thermoplastic polymers. Studies, such as that conducted by Guo et al. [11], have demonstrated notable enhancements in mechanical properties by incorporating CB. For instance, they found that the UTS of CB/PLA composites increased by nearly 10% with a 12% CB reinforcement. These findings underscore the potential for carbon-based filler materials to improve the mechanical properties of thermoplastic composites significantly. Polymer-based materials exhibit time-dependent behavior due to the nature of viscoelasticity, in contrast to the instantaneous response of elastic materials. One notable characteristic of this behavior is creep, where viscoelastic materials experience an increase in deformation over time when subjected to a constant load. This phenomenon underscores the importance of careful consideration in design for long-term applications. Zhang et al. [12]

conducted a study to investigate the creep dynamics of PEI, especially its alteration with the introduction of reinforcements. By incorporating varying concentrations of short carbon fibers (SCF) into PEI, they noted a reduction in creep deformation as SCF concentration increased. Similarly, Panin et al. [13] studied the cyclic creep characteristics of PEI with SCF reinforcement. Their findings indicated a diminishing creep rate with the increasing length of SCF, with a reported 4.5-fold reduction compared to neat PEI at 2000 μm. Despite these investigations in literature, the comprehensive understanding of the creep behavior of PEI composite parts, especially manufactured via FFF, remains relatively unexplored. Understanding the creep behavior of polymeric composites and predicting their future performance relies not only on experimental research but also on mathematical modeling and simulation. Theoretical models enable us to comprehend materials' creep behavior better and predict their potential performance by supporting experimental data. Various viscoelastic models, such as the Burgers model, generalized Maxwell or Kelvin models, Zener model, and Findley's empirical model, are commonly used to simulate experimental creep data [14]. In a study conducted by Xu et al. [15], the creep behavior of chopped bagasse fiber-reinforced polyvinyl chloride (PVC) and high-density polyethylene (HDPE) composites was successfully simulated using the Burgers model and Findley power-law model. These models provided results consistent with experimental data, accurately describing the creep properties of the materials. Another point is evaluating the material's service life and structural integrity over time, especially when designing parts that will be used over a long period. However, such a long-term test is unfeasible to be performed on a lab scale. Therefore, the Time-Temperature Superposition Principle (TTSP) facilitates estimating the life of a material by creating long-term creep data and manipulating the short-term creep data [13]. Jabbar et al. [16] used TTSP to simulate the long-term creep behavior of jute fiber-reinforced epoxy composites using short-term creep data. Since the regular Arrhenius model cannot adequately model PEI, which exhibits a complex viscoelastic behavior, Wu et al. [17] modified the Arrhenius model to succesfully simulate PEI's viscoelastic properties.

1.3 Hypothesis

Due to the nature of the production methodology, the mechanical properties of FFF parts are lower than the conventional manufactured counterparts. For this reason, FFF parts cannot compete with parts produced by conventional methods in advanced engineering applications. To enable the integration of 3D-printed parts into such industries, it becomes essential to address this deficiency in mechanical attributes, aiming to elevate them to a level that matches injection-molded parts.

Incorporating varying concentrations of CB into PEI-based 3D-printer filaments is hypothesized to enhance the mechanical properties of parts fabricated through FFF significantly. As the concentration of CB increases, there is expected to be a proportional improvement in printed parts' mechanical properties, particularly creep behavior. Furthermore, it is anticipated that the enhanced mechanical properties achieved through the CB reinforcing will enable PEI-based 3D printed parts to meet and potentially exceed the performance of conventionally manufactured components. This unlocks their potential for utilization as structural and functional elements in demanding applications, such as the aerospace and defense industry. In addition to experimental investigations, mathematical modeling provides an understanding of the creep properties of PEI-based composites, allowing more accurate prediction of their long-term performance under load.

To test this hypothesis, a systematic experimental approach will be undertaken, involving the fabrication of composite 3D printer filaments with varying concentrations of CB. These filaments will then be used to produce test specimens through FFF, and their thermal, rheological, and mechanical properties will be comprehensively characterized. In addition to experimental investigations, linear viscoelastic functions in literature will be employed to gain insights into the creep behavior of the polymeric composites.

2. FFF WITH HIGH-PERFORMANCE THERMOPLASTICS

AM is defined as a manufacturing method of joining materials, generally layer by layer, to create parts from 3D model data [18]. Initially introduced in the mid-1980s as a technology called "rapid prototyping" for the production of models and prototype parts [19], it has since undergone continuous development. The increase in production speed, part quality, dimensional accuracy, and the variety of usable feedstock materials has led to widespread adoption of AM technologies. Due to its numerous advantages over conventional manufacturing methods, AM has evolved beyond rapid prototyping and found applications in various fields. This evolution has standardized the term "additive manufacturing," commonly referred to as "3D printing" technologies in everyday life [20].

Conventional manufacturing methods are generally classified as subtractive, casting, and forming technologies. In subtractive manufacturing technologies, a block of raw material is shaped into the desired product by removing excess material using cutting tools. Although this method can produce highly precise products, it results in approximately 90% of the raw material being wasted and rendered unusable [21]. In contrast, AM technologies build objects by adding material layer by layer, as suggested by the term "additive." This method offers significant advantages: it allows the construction of objects with complex internal geometries and the creation of functional parts without the need for assembly, thereby reducing production time, cost, and material waste [22]–[24].

Consequently, AM technologies are utilized across numerous industries and application areas, including aerospace [25], automotive [26], medical [27], and consumer products [28], and holds the potential for even broader applications in the future [29,30].

2.1 Overview of the FFF Process

FFF is one of the most widely used AM technologies across various sectors, including biomedical, aerospace, automotive, electronics, and construction, as well as within the scientific community. Its leading position in the polymer 3D printing market is attributed to design flexibility, low cost, easy accessibility to FFF printers and lower entry barriers [31]. The FFF method based on the deposition of melted thermoplastic material layer by layer onto a building platform, extruded from a nozzle. The basic working principles of an FFF system are as follows (see Figure 2.1):

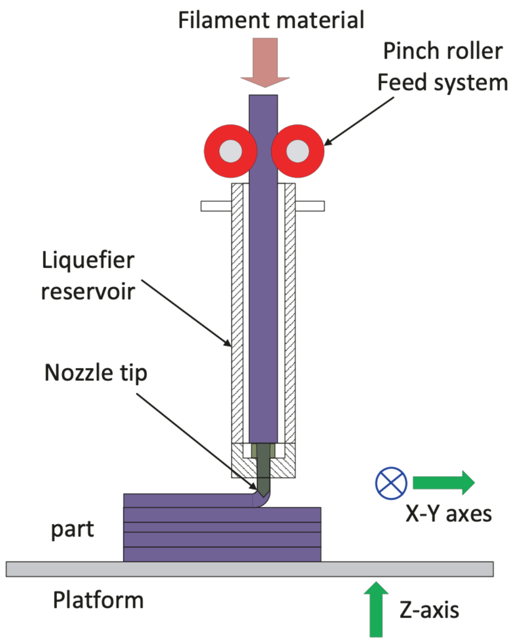

Figure 2.1 : 3D printing process schematic with FFF method [1].

- Filament Feeding: The polymer raw material in filament form is fed into the system through a pinch roller feeding mechanism. The pinch roller controls the filament, feeding it at a consistent rate and speed.
- Liquifier Reservoir: The filament enters the liquefier reservoir from the feeding mechanism. Inside the reservoir, heating elements melt the filament. At this stage, the temperature of the filament is carefully controlled to achieve an appropriate viscosity of the melt.

- Extrusion: The liquefied filament in the reservoir is pushed towards the nozzle tip. The nozzle ensures that the melted filament is extruded in a thin, controlled manner. The extruded filament is deposited onto the build platform in cylindrical roads called beads.

- Print Head Movement: The movement of the print head within a printing environment is enabled by stepper motors, which typically operate in the XY plane. These motors precisely control the nozzle's position, allowing each layer's geometry to be accurately formed.

- Layer-by-Layer Building: Once a layer of the part is completed, the build platform moves along the Z-axis, transitioning to the next layer. Each new layer fuses with the one below, ensuring the mechanical integrity of the part.

- Cooling and Solidification: The extruded filament, upon being deposited onto the build platform, cools and solidifies rapidly. This quick cooling helps ensure strong adhesion between the layers and enhances the overall durability of the part.

2.2 FFF Materials

Different types of polymers for FFF applications can be employed depending on requirements. These polymers are classified on a pyramid based on their mechanical properties, operating temperatures, and cost (see Figure 2.2) [32]. While the bottom of the pyramid, commodity thermoplastics such as ABS, PLA, HDPE, etc. employ a wide range of commercial applications, on top of the pyramid shown in Figure 2.2, high-performance thermoplastics can meet high strength demands. They possess distinct properties compared to commodity and engineering thermoplastics, including higher melting and glass transition temperatures, elevated molecular weight, and increased entanglement ratio. These properties confer superior characteristics such as enhanced thermal stability, elevated chemical resistance, and the capability to retain mechanical properties at high temperatures.

Recent research reports that the use of the FFF method is accelerating in advanced technological applications, due to the availability of high-performance thermoplastics. The most popular high performance thermoplastics in FFF applications are PEI,

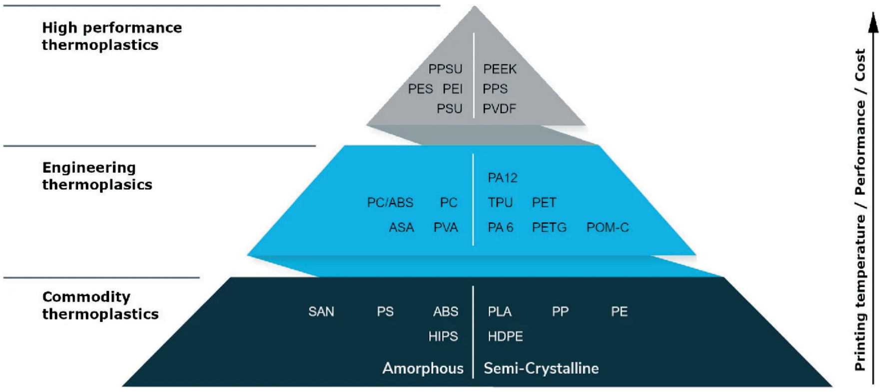

Figure 2.2 : Classification of thermoplastic polymers for FFF applications [32].

PEEK, Polyphenylsulfone (PPSU), Polyphenylene sulfide (PPS), etc. These advanced materials offer enhanced properties and performance, expanding the scope of applications for FFF technology in industries requiring robust and durable components [7,8,33].

PEI is a high-performance thermoplastic polymer renowned for their exceptional mechanical properties and chemical resistance. PEI possesses a unique chemical structure characterized by aromatic imide, propylidene, and ether groups, imparting stiffness and processability to the material. With high mechanical strengths and rigidity at varying temperatures, PEI finds applications in the aerospace, automotive, and electronics industries. Since it exhibits linear stress-strain relationships and is exceptionally resistant to creep at high temperatures, it can replace metal parts in some structural applications. Its resistance to a wide range of chemicals, coupled with low molding shrinkage and excellent flame resistance. Moreover, PEI's high softening point and elevated heat deflection temperature make it an ideal candidate for high-temperature environments [34]. Its increasing adoption in structural components, such as aircraft cargo flooring and business jet interiors, reflects its growing prominence in advanced engineering applications [35].

3. LINEAR VISCOELASTIC MODELS FOR CREEP

Some materials, such as thermoplastic polymers, can display characteristics of both elastic solids and viscous liquids when subjected to an applied load. Elastic materials deform instantaneously upon applying a load and return to their original shape once the load is removed. Viscous materials, on the other hand, deform depending on time under stress and maintain their deformed state even after the load is removed. As the name suggests, viscoelastic materials simultaneously exhibit elastic and viscous characteristics. When a load is applied to a viscoelastic material, such as a polymeric material, its deformation increases over time, unlike an elastic material. This behavior arises from molecular rearrangement within the material. The applied mechanical stress induces position change of the long polymer chains. After removing the load, the polymer returns to its original form [36].

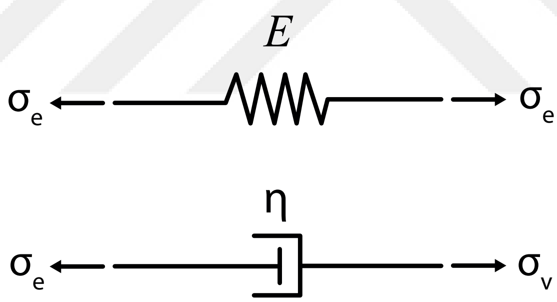

Figure 3.1 : Representation of the linear spring and dashpot.

Understanding the viscoelastic behavior of materials has practical implications in various fields, from material science to engineering. Various mechanical models have been developed to model this behavior. These models, which combine a linear spring representing elastic behavior and a dashpot representing viscous behavior, have tried to explain the stress-strain relations of viscoelastic materials. These models are limited to describing only linear viscoelasticity, which applies to polymer systems undergoing small deformations, and Boltzmann's superposition principle can be applied as in elastic solids [37,38]. Figure 3.1 illustrates the linear spring and dashpot, and the corresponding stress-strain relations are given in Eq. 3.1 and 3.2.

$$\sigma_e = E \times \varepsilon_e \tag{3.1}$$

$$\sigma_v = \eta \times \dot{\varepsilon}_e \tag{3.2}$$

Here, σ denotes applied stress, and ε represents captured strain, with E and η denoting stiffness and viscosity coefficients, respectively. The sub-indices e and v define elastic and viscous behavior.

3.1 Maxwell Model

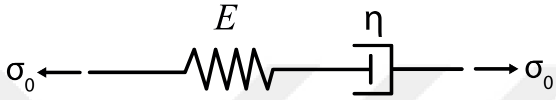

Figure 3.2 : Representation of the Maxwell model.

The Maxwell model in Figure 3.2 consists of a linear spring and a dashpot connected in series. The linear spring represents the instantaneous strain when the load is applied, while the dashpot represents the permanent strain. The total strain and stress in the Maxwell model are expressed in Eq. 3.3 and 3.4.

$$\sigma = \sigma_e = \sigma_v \tag{3.3}$$

$$\varepsilon = \varepsilon_e + \varepsilon_v \tag{3.4}$$

Similarly, total strain rate is written as

$$\dot{\varepsilon} = \dot{\varepsilon}_e + \dot{\varepsilon}_v \tag{3.5}$$

Substituting Eq. 3.1 and 3.2 in Eq. 3.5, the total strain in the Maxwell model is obtained as Eq. 3.6

$$\dot{\varepsilon} = \frac{\dot{\sigma}}{E} + \frac{\sigma}{\eta} \tag{3.6}$$

This equation is written in differential form as Eq. 3.7 and 3.8, referred to as the governing equation for the Maxwell model.

$$\frac{d\dot{\varepsilon}}{dt} = \frac{1}{E}\frac{d\sigma}{dt} + \frac{\sigma}{\eta} \tag{3.7}$$

$$d\dot{\varepsilon} = \frac{1}{E}d\sigma + \frac{\sigma}{\eta}dt \tag{3.8}$$

A constant stress, σ_0, is applied during the creep test. Integrating Eq.3.8, the time-dependent strain response of the Maxwell model is expressed by the governing equation in Eq. 3.9 and 3.10.

$$\int_0^t d\varepsilon = \frac{1}{E}\int_0^t d\sigma + \frac{\sigma_0}{\eta}\int_0^t dt \tag{3.9}$$

$$\varepsilon(t) = \frac{\sigma_0}{E} + \frac{\sigma_0}{\eta}t \tag{3.10}$$

Based on this governing equation, the strain response of the Maxwell model under constant σ_0 load: An instantaneous strain occurs due to the linear spring when the load is applied, followed by linearly increasing strain due to the damping increasing linearly until t_1. When the load is removed from the system (after t_1), the instantaneous strain of the linear spring is fully recovered, i.e., the spring is 100% restored. Still, the viscous strain represented by the dashpot is a permanent deformation and cannot be recovered. Hence, the Maxwell model fails to capture viscoelastic recovery, only simulating the elastic recovery of the system [39].

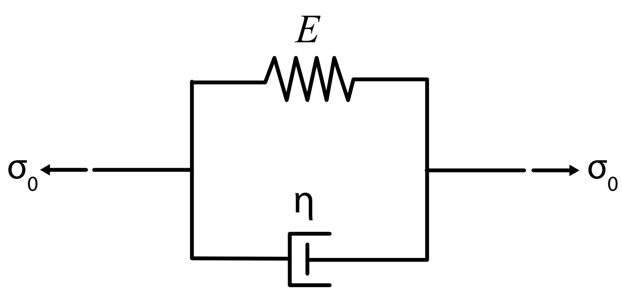

Figure 3.3 : Representation of the Kelvin-Voigt model.

3.2 Kelvin-Voigt Model

In the Kelvin-Voigt model, the linear spring and dashpot are connected in parallel, as illustrated in Figure 3.3. Total stress and strain in this model are articulated in Eq. 3.11 and 3.12.

$$\sigma = \sigma_e + \sigma_v \tag{3.11}$$

$$\varepsilon = \varepsilon_e = \varepsilon_v \tag{3.12}$$

Substituting Eq. 3.1 and 3.2, the total stress equation for the Kelvin-Voigt model is derived as in Eq. 3.13

$$\sigma = E\varepsilon + \eta\dot{\varepsilon} \tag{3.13}$$

Eq. 3.13 is a first-order differential equation, finds its solution by assuming $\sigma = \sigma_0$ in the creep test:

$$\varepsilon(t) = \frac{\sigma_0}{E} + A.exp\left(-\frac{E}{\eta}t\right) \tag{3.14}$$

To determine the unknown coefficient A in 3.14, assuming no initial strain in the system ($\varepsilon_{t=0} = 0$), the strain response of the Kelvin-Voigt model is obtained as in Eq. 3.15:

$$\varepsilon(t) = \frac{\sigma_0}{E}\left[1 - exp\left(-\frac{E}{\eta}t\right)\right] \tag{3.15}$$

The strain response of the Kelvin-Voigt modeled with Kelvin-Voigt function successfully in Eq. 3.15. It is evident that the strain undergoes exponential growth upon applying a constant load, σ_0. Following the loading phase, the strain gradually decreases and tends to return to zero. However, it's important to note that the Kelvin-Voigt model cannot represent the instantaneous strain resulting from bond stretching. Furthermore, it fails to simulate permanent (viscous) deformations that may persist in the system.

3.3 The Burgers Model

The Burgers model, also known as the four-element model, has been widely used in the literature to model viscoelastic properties of materials such as creep [40,41]. As shown in 3.4, the Burgers model is constructed by connecting a Maxwell and a Kelvin-Voigt unit in series [42,43]. By combining these two models, it is thought that the shortcomings of both models can be overcome and show the elastic and viscous parts of viscoelastic materials, constituting a more appropriate model [44]. The literature has reported that the Burgers model successfully simulates viscoelastic behavior. In the Burgers model, the total strain on the material at time t under stress σ_0 equals the sum of the strains of the Maxwell and Kelvin-Voigt units (see Eq. 3.16 and 3.17).

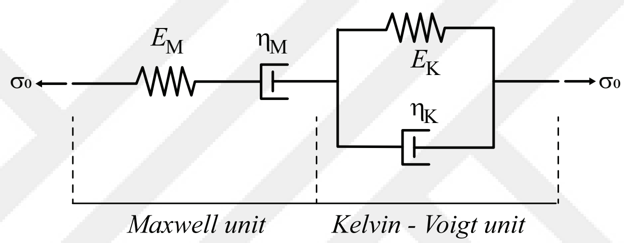

Figure 3.4 : Representation of the Burgers model.

In the equation of the Burgers model (3.17), σ_0 represents the applied constant stress; E_M and η_M represent the Maxwell spring elastic modulus and Maxwell dashpot viscosity, respectively; E_K and η_K represent the Kelvin-Voigt spring elastic modulus and Kelvin-Voigt dashpot viscosity, respectively.

$$\varepsilon_B = \varepsilon_{M,spring} + \varepsilon_{M,dashpot} + \varepsilon_K \tag{3.16}$$

$$\varepsilon_B = \frac{\sigma_0}{E_M} + \frac{\sigma_0}{\eta_M} t + \frac{\sigma_0}{E_K} \left[1 - \exp\left(-\frac{E_K}{\eta_K} t \right) \right] \tag{3.17}$$

3.4 Findley's Power-Law Model

Another model used to characterize viscoelastic behavior is Findley's empirical power law method. Findley's power law equation, expressed by 3.18, is widely used in the literature to predict the creep of viscoelastic materials [45]–[47]. In this equation, ε_0

represents the instantaneous elastic strain as a function of time and temperature, and A and n represent the experimentally obtained material constants.

$$\varepsilon = \varepsilon_0 + At^n \tag{3.18}$$

3.5 Generalized Kelvin-Voigt Model

The last model used in this study is the generalized Kelvin-Voigt model. This model consists of a Kelvin-Voigt unit connected in n number of series. In addition, a Maxwell spring is added at the beginning of this series to represent elastic deformation. The equation of the generalized Kelvin-Voigt model is shown in Eq. 3.19

$$\varepsilon_K = \frac{\sigma_0}{E_0} + \sum_{i=1}^{n} \frac{\sigma_0}{E_n}\left[1 - \exp\left(-\frac{E_n}{\eta_n}t\right)\right] \tag{3.19}$$

The number of Kelvin-Voigt terms n shown in the equation is determined according to the material's behavior. This study used the Kelvin-Voigt model with three terms $(n = 3)$

3.6 TTSP

Determining the long-term creep behavior of polymer composites intended for structural applications ensures their performance over time. However, one of the primary challenges in assessing long-term creep behavior lies in the long test durations. To address this challenge, models can be employed to predict long-term creep behavior based on short-term experimental data. One well-established creep prediction model is the TTSP, which establishes an equivalence between the material's behavior at elevated temperatures and its long-term behavior at a relatively lower constant temperature [48,49]. To create a long-term creep master curve for a material, short-term creep tests are conducted at increasing temperatures and plotted on a logarithmic scale. The reference curve is held constant while all other curves are moved along the time axis using a shift factor, $log\ a_T$ until they are superimposed.

The shift factor, $log\ a_T$, which determines the amount of shifting of the curves in TTSP, has been calculated using different methods in the literature. One of these methods, the William-Landel-Ferry (WLF) empirical equation, was shown in Eq. 3.20 [50].

$$loga_T = \frac{C_1 * (T - T_{ref})}{C_2 + (T - T_{ref})} \tag{3.20}$$

In Eq. 3.20, the coefficients C_1 and C_2 represent the material-specific constants, T_{ref} is the reference temperature in the shift, and T is the temperature.

The Arrhenius equation (see Eq. 3.21) governs chemical reaction rates as a function of temperature. Integrating the Arrhenius equation and incorporating it into TTSP can provide a powerful framework for predicting the long-term creep behavior of materials over their service life. The creep factor can be defined below the T_g using an Arrhenius law.

$$loga_T = \frac{E_a}{2.303R}\left(\frac{1}{T} - \frac{1}{T_0}\right) \tag{3.21}$$

Where E_a is the activation energy, R is the universal gas constant and T_0 is a reference temperature in Kelvin [49]. Indeed, alongside the WLF and Arrhenius, the creation of a master curve by manually shifting the creep data to achieve superimposed a single curve is another method reported in the literature for creep estimation. This approach allows researchers to tailor the TTSP model to better suit the specific characteristics of the material under consideration, resulting in more precise predictions of its creep behavior. By manually aligning the experimental data, researchers can account for nuances and complexities in the material's response to different temperature and time conditions, ultimately improving the reliability of the creep estimation process [12].

Alongside these methods, various studies in the literature have explored different approaches to the shift method [17,51]. One such approach is the MNAT procedure developed by Naya et al. [52], which aims to predict the mechanical properties of viscoelastic materials. The procedure involves the following steps:

1. Generating curves that represent the selected viscoelastic property against frequency at each temperature.

2. Applying a non-parametric regression model known as b-spline to fit each curve, using the `mgcv` library available in the statistical software R.

3. Creating smooth estimates for each curve, consisting of 3,000 equally spaced fitted points across the frequency range, using these flexible models.

4. Performing numerical differentiation on each curve obtained in the previous step, utilizing the `sfsmisc` library in R.

5. Selecting a reference temperature to construct the master curve.

6. Determining horizontal shifts by aligning the derivatives of these shifts with the derivatives of the horizontal displacements. This is achieved by measuring the L1 distances between the derivatives at adjacent temperatures, resulting in the master curve through an iterative process.

7. If required, calculating vertical shifts by measuring the L1 distances between the horizontally shifted curves.

8. Fitting the master curve using b-spline non-parametric models, with the accuracy of the master curve being validated through bootstrap confidence intervals at a 95% confidence level.

To facilitate the use of this method for obtaining TTSP curves, Meneses et al. [51] developed a library in R. By leveraging this library, experimentally obtained strain (or compliance) curves at different temperatures can be analyzed within the TTS framework. Additionally, the library supports the use of WLF and Arrhenius approaches.

4. MATERIALS AND METHODS

4.1 Materials

PEI in granule form (commercially known as ULTEM 1010) was purchased from Sabic as a matrix polymer to fabricate composite filaments. PEI has a 1.27g/cm^3 density and a T_g of 217 °C. CB (with a density of 1.90 g/cm^3) from OMSK carbon was employed as a reinforcement material. All materials were used without treatment.

4.2 Composite Production

Since PEI is a polymer that retains moisture, it's essential to eliminate any residual moisture before the filament production process. This moisture can lead to air bubbles in the filament during extrusion. The PEI granules were placed in a convection oven (Nüve KD 400) at 150 °C for eight hours to remove the residual moisture, allowing the moisture to evaporate effectively.

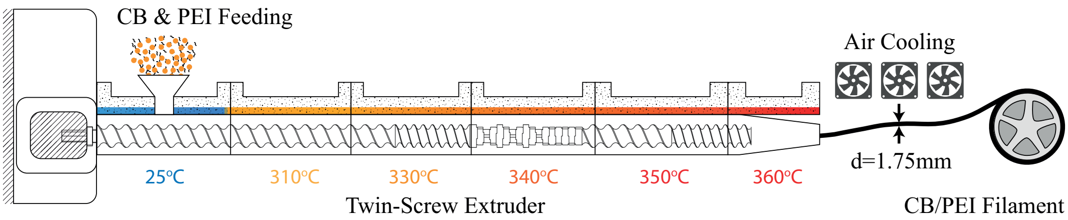

Figure 4.1 : Illustration of the extrusion process details of CB/PEI filaments.

The neat PEI and CB-reinforced PEI composite filaments were fabricated using a custom-built twin-screw extruder. The extruder, tailored explicitly to high-performance polymers, was designed and manufactured by Kokbir Import & Export. The extrusion unit consists of two co-rotating screws with a screw diameter (D) of 12 mm and a length (L) of 264 mm, resulting in a L/D ratio of 22. It also consists of six different mixing zones (individually controlled temperatures) whose screw designs are configured to ensure homogeneous mixing of the reinforcement material in the matrix without agglomeration. Further details of the screw configuration are given in the previous study [6].

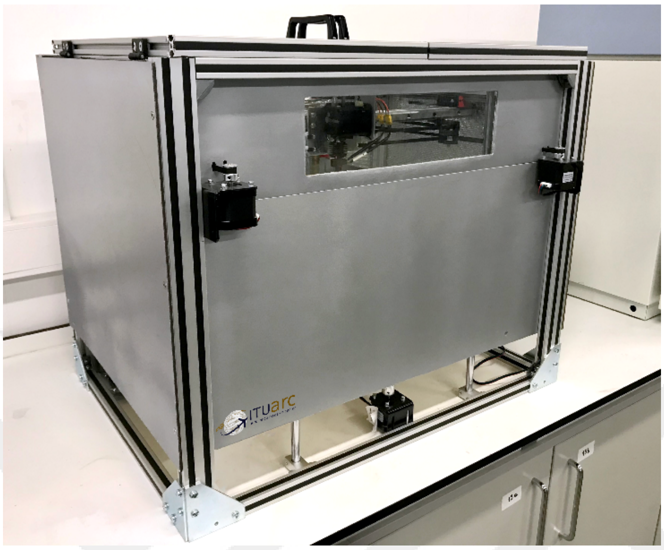

Figure 4.2 : 3D printer called "Pegasus" suitable for printing high-performance thermoplastics.

Neat PEI and 5, 10, and 20 wt% CB reinforced PEI filaments with a diameter of 1.75 mm, which is suitable for 3D printers, were produced using process parameters of temperature zones of 310-360 °C from the hopper to the die and 210 rpm screw rotor speed. To achieve the desired CB ratio in the production of CB-reinforced filaments, first, CB was manually mixed into PEI granules and fed as a mixture from a single hopper. This approach was favored over feeding the CB through the side feeder due to challenges encountered during mixing ratio optimization. Attempts to optimize the screw speed of the side feeder to obtain the desired mixing ratio proved unsuccessful, primarily because the CB flowed too rapidly through the hopper. The filament extruding process illustrated in Figure 4.1.

4.3 Creep Test Samples Preparation

Following ASTM D790–17 standards, neat PEI and CB/PEI DMA samples were printed using a 3D printer to print high-performance thermoplastics (ARC-Pegasus

Table 4.1 : 3D-Printing parameters of Creep Test Samples

Parameter (unit)	Value
Nozzle Temperature (°)	375 (Neat PEI) 380 (5 wt% CB/PEI) 385 (10 wt% CB/PEI)
Bed Temperature (°)	150
Nozzle diameter (mm)	0.4
Layer height (mm)	0.2
Number of layers	15
Infill pattern	Rectilinear pattern (-45°/+45°)
Infill ratio	100%
Number of perimeters	3
Skirt (1^{st} layer)	10 outlines without offset
Speed (mm/s)	30 (50% reduced for 1^{st} layer)

(see Figure 4.2) [9]). Printing parameters were tabulated in Table 4.1. Although neat PEI and 5, 10 wt% CB/PEI samples were successfully produced, the 20 wt% CB-reinforced PEI filament proved challenging for successful 3D printing. Increased CB ratio induced stress concentration zones, producing exceedingly brittle filaments. Hence, continual breakage occurred during printing attempts. The obtained granules, filaments, and creep test specimens were shown in Figure 4.3 as representative.

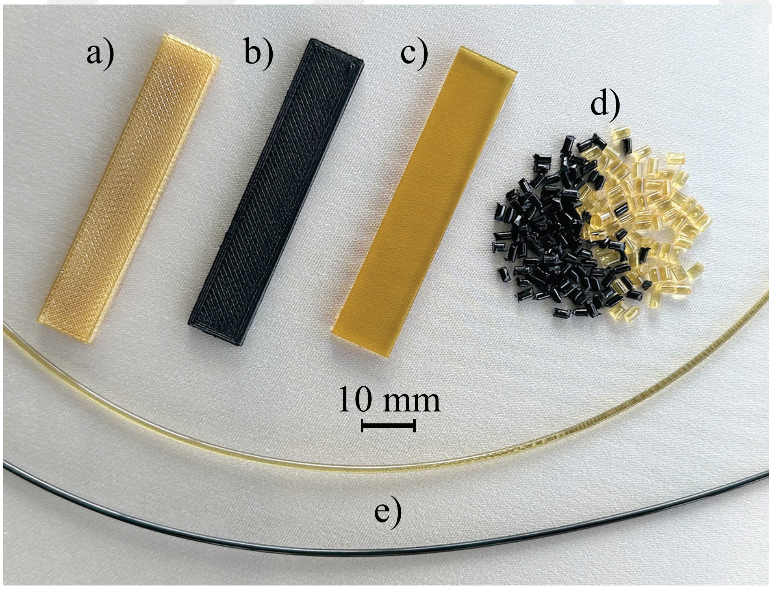

Figure 4.3 : Representative samples of a) 3D printed Neat PEI and b) 3D printed 5 wt% CB/PEI, and c) Hot-pressed (HP-) Neat PEI DMA Samples; and Neat PEI and 5 wt% CB/PEI d) granules and e) filaments.

4.4 Characterization

4.4.1 Thermogravimetric analysis (TGA)

All CB/PEI composite filament samples were subjected to a thermogravimetric analysis (TGA) using TA Instrument-TGA55 to investigate their thermal properties. Samples weighing 9-11 mg were cut off from filaments and heated at 10 °C/min of 30 °C-700 °C with a nitrogen purge of 50 mL/min to determine the thermal decomposition temperature. Temperature-induced weight loss was monitored and analyzed.

4.4.2 Oscillatory rheology analysis

Oscillatory rheology analyses were conducted to understand better how reinforcement influences polymer microstructure change and viscoelastic behavior. Before testing neat PEI and CB/PEI granules, they were preconditioned in an oven at 150 °C. They were then tested on TA Discovery HR-2 rheometers in parallel plate geometry with 1 mm gaps and 25 mm diameters. A strain sweep test was conducted at 360 °C with an angular frequency of 10 rad/s between 0.0125% and 12.5% strain to determine the linear viscoelastic regions (LVR) boundaries. All specimens within the LVR at 360 °C were then subjected to frequency sweep tests between 0.1 and 628 rad/s.

4.4.3 Scanning electron microscopy (SEM)

A scanning electron microscope (FEG-SEM) (Quanta FEG 450) operated at 15 keV was employed to characterize the dispersion and distribution of CB particles in the polymer matrix. Gold-palladium alloys were coated to the cross-sectional areas of CB/PEI filaments after fracturing in liquid nitrogen.

4.4.4 Filament tensile test

The mechanical properties of neat PEI and 5, 10, and 20% CB/PEI composites were investigated by filament tensile testing. The tests were carried out at room temperature using a SHIMADZU AGS-X universal testing machine (UTM) with a single-bollard, self-tightening type grips with 1 kN load cell at room temperature. According to

ASTM D-3822 [53], a crosshead speed of 5 mm/min was applied without using an extensometer and the specimen length was 1050 mm with a gauge length of 200 mm. Moreover, each of the tests was repeated with three samples.

4.4.5 Creep test

Within this thesis, creep tests were conducted using dynamic mechanical analysis (DMA) device (TA Instrument DMA 850, New Castle, DE). The creep tests were realized using two different protocols. In the first protocol:

- Creep tests were carried out under the dual cantilever fixture.
- Specimens fabricated using neat PEI, 5 wt% CB/PEI, and 10 wt% CB/PEI filaments were tested.
- In the creep tests, a constant stress of 4 MPa was applied for a duration of 15 minutes followed by a recovery period of 15 minutes during which the load was removed. This procedure was repeated at every 20 °C interval within the temperature range of 30 °C to 170 °C.
- Before the creep tests, a strain sweep tests was performed at 170 °C, the highest temperature to be applied, to determine the applied stress (4 MPa) remaining within the Linear Viscoelastic Region (LVR).

In the second set of experiments, the creep tests conducted with several modifications to the test protocol:

- Previously, only one specimen of each CB composition was tested, which could compromise the accuracy and reliability of the results, especially considering the variability inherent in composite materials and additive manufacturing. Therefore, the creep tests were repeated using three specimens of each composition.
- Creep tests were also performed on neat PEI hot-pressed specimens to facilitate comparing the mechanical properties of additively manufactured parts with those produced using conventional manufacturing methods.

- The fixture was replaced with a three-point bending fixture to address the issue of increased specimen deformation due to extra moments when using a dual cantilever fixture.
- In previous creep tests, 170 °C was chosen as the limit temperature. However, PEI could still maintain stiffness at this temperature without significantly decreasing mechanical strength values. Therefore, the temperature was increased to 190 °C to further challenge the material.
- The TA Instrument DMA 850 is designed to apply a maximum stress of 4 MPa. However, in previous tests where a 4 MPa creep stress was selected, it was observed that the instrument could not consistently apply exactly a 4 MPa load. As a result, the applied test stress was reduced to 3 MPa.
- To optimize testing efficiency, the test time at each temperature was reduced from 900 to 600 sec. while still ensuring sufficient data collection.

The creep strain curves of all specimens at different temperatures were analyzed using the nonlinear curve fitting module of OriginPro software. Burgers, Findley power-law, and generalized Kelvin-Voigt models were used, and the relevant parameters were defined in the software. The initial and boundary values were carefully set to guarantee the convergence of the curve-fitting process. The parameters obtained from the models for each creep curve were then used to establish a correlation with the experimental conditions.

Two different methods were tried to obtain the creep master curves of composites using the time-temperature superposition principle. As mentioned in Section 3.6, the TTS R library was used in the first method, which was obtained using the MNAT procedure developed by Naya et al. [52] and includes the WLF and Arrhenius methods. The second method used Python to write a code to manually shift each temperature curve along the horizontal and vertical axis. The creep master curves of neat PEI, hot pressed PEI, 5 wt% CB/PEI, and 10 wt% CB/PEI were generated by two different methods.

5. RESULTS AND DISCUSSION

5.1 TGA

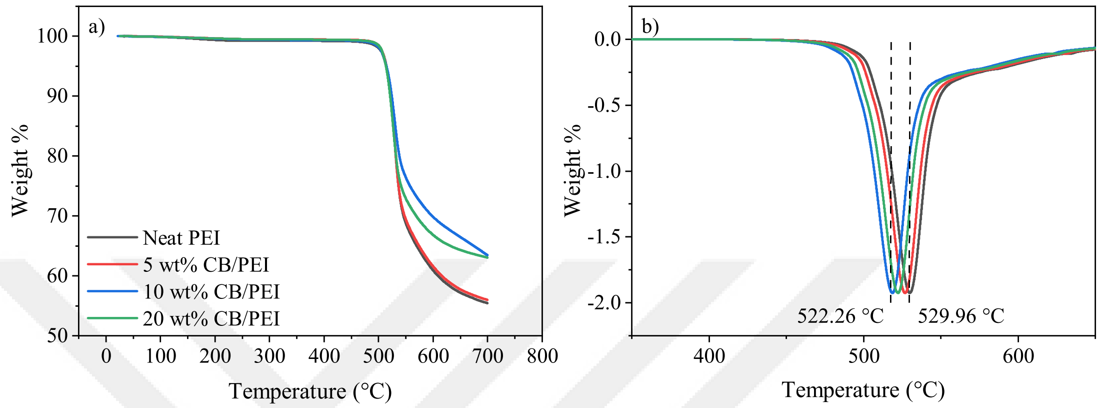

Figure 5.1 : TGA curves of neat PEI and 5, 10, and 20 wt% CB/PEI granules.

PEI, a thermoplastic polymer, features aromatic imide, propylidene (isopropylidene), and ether groups within its chemical structure. The aromatic imide group contributes to PEI's high thermal stability and stiffness. Conversely, the ether group facilitates easy processability and lowers melt viscosity [54]. Two distinct mechanisms are observed in the degradation of aromatic polymers like PEI: crosslinking and chain scission. Crosslinking, prevalent at approximately 380 °C in PEI, is the primary degradation mechanism, enhancing molecular mass and strength. Beyond 400 °C, chain scission becomes dominant, exhibiting a peak decomposition rate around 510-540 °C [55,56]. Temperature-dependent weight loss variation was observed to investigate the effect of CB reinforcement on PEI's thermal stability behavior and decomposition temperature. Figure 5.1 shows the corresponding TGA and their derivative thermogravimetric (DTG) curves of neat PEI, 5, 10, and 20 wt% CB/PEI. All samples were exposed up to 700 °C, which is above the range of the chain scission thermal degradation regime for the PEI.

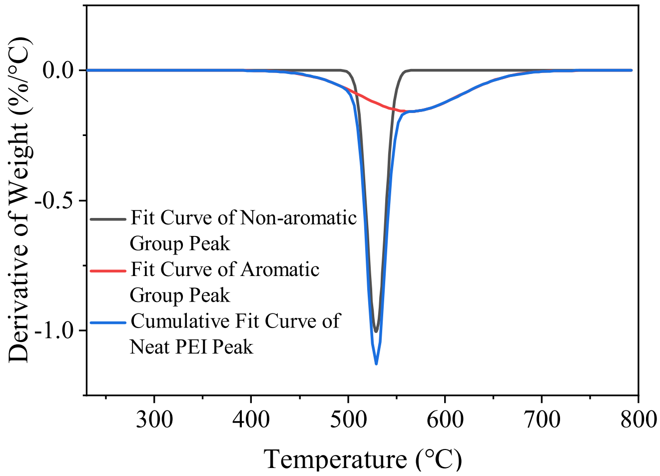

Figure 5.2 : TGA curves of neat PEI and 5, 10, and 20 wt% CB/PEI granules.

Table 5.1 : Onset and the maximum thermal decomposition temperatures of the samples depending on the CB amount.

CB Concentration (wt%)	T_{onset} °C	T_{max} °C
Neat	515.05	529.96
5	514.29	526.91
10	511.13	518.67
20	512.24	522.26

Additionally, a detailed examination of the samples' DTG curves revealed a two-stage chain scission process, which is proved by the peak analysis in Figure 5.2. The primary decomposition step occurs around 529 °C, followed by a secondary step at 564 °C. The first stage is attributed to the scission of ether bridges and the breaking of imide rings, whereas the second stage pertains to the degradation of the stronger aromatic groups [6,54].

TGA results for neat PEI and CB-reinforced PEI indicate no measurable weight loss up to 500 °C, similar to the literature [56]. The initial thermal decomposition temperatures, T_{onset}, and the temperature at the maximum rate of thermal decomposition, T_{max}, for neat PEI and 5, 10, 20 wt% CB reinforced PEI composites, respectively. As a result, it was observed that CB did not cause a significant change in the thermal degradation temperature of PEI, indicating that CB reinforcement has no significant effect on the thermal stability of PEI. Similar results were also observed in the [57].

5.2 Oscillatory Rheology Analysis

Reinforcing materials need to be uniformly dispersed in the polymer matrix to enhance polymeric parts' performance effectively. However, observing the reinforcement dispersion state within the matrix material is not straightforward, as in-situ observations yield local results. The importance of oscillatory rheology analysis is evident here. It is an effective tool for investigating the dispersion quality of CB in the PEI matrix, providing insights into the microstructure that evolves with the addition of reinforcement to the system and assessing the formation of the filler-matrix interactions.

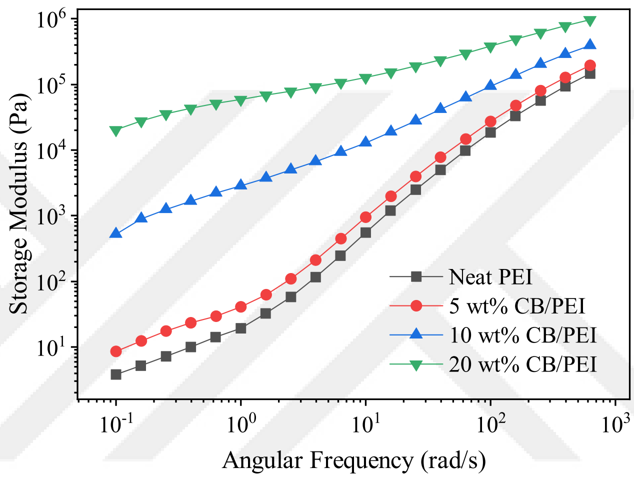

Figure 5.3 : Storage modulus curves as a function of the angular frequency of neat PEI and CB/PEI composites.

Oscillatory rheology measurements were performed for neat PEI and 5, 10, and 20 wt% CB/PEI composite samples. Figure 5.3 shows the storage modulus results for all samples as a function of angular frequency. The storage modulus, representing the composite stiffness and elastic behavior, is a key indicator. When the storage modulus trend of neat PEI is examined, it exhibits a frequency-dependent, typical polymer behavior. This behavior was observed at 5 wt% CB concentration. However, frequency-dependent behavior was reduced when it reached 10 wt% CB concentration. At his concentration, 10 wt% CB/PEI transitioned from a liquid-like behavior to a more solid-like behavior (Hooken behavior), indicating that microstructure began to change. At 20 wt% CB fraction, an almost frequency-independent storage modulus behavior was observed. These findings are similar to those reported in the literature.

Kalaitzidou et al. measured the storage moduli of CB-reinforced polypropylene composites at different ratios, and at 20 wt% CB, the storage modulus became almost frequency-independent [58].

The impact of CB reinforcement on the storage modulus is best understood when evaluated separately in the low-frequency and high-frequency regions. High reinforcement loading (10 wt% CB and above) significantly increases the storage modulus at low frequencies (up to 1 rad/s), indicating enhanced stiffness and elastic behavior. However, this effect diminishes at high frequencies, suggesting that the CBs do not significantly influence the short-range dynamics of the PEI chains. Similar results are seen in other rheology studies [59,60]. This behavior implies that while the interactions between the filler matrix are pronounced at low frequencies (long-range motion), i.e., CB restricts the motion of polymer chains, they are weak at high frequencies. It physically means that the presence of CB can effectively prevent large-scale polymer chain relaxations, so it can be employed to increase the stiffness of the PEI at low frequencies [61]. In the literature, it has been proposed that the carbon black (CB) effect weakens in comparison to the entanglement length at length scales or chain slippage at high frequencies could be responsible for this phenomenon [61]–[63].

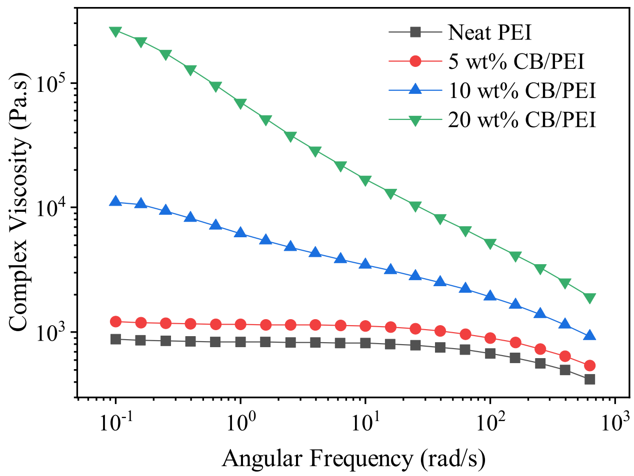

Figure 5.4 : The complex viscosity curves of neat PEI and CB/PEI composites as a function of the frequency.

Complex viscosity is the other rheological property used to evaluate the reinforcement effect and frequency-dependent behavior. As seen in Figure 5.4, the presence of CB reinforcement had an incremental effect on complex viscosity, and PEI becomes more viscous with increasing CB contents at the low-frequency region (up to 1 rad/s). Similar to storage modulus results, this point is related to the particle network formed within the composite that restrains molecular motion in the long range, resulting in high viscosity. However, this effect gradually decreases with increasing frequency as a result of shear-thinning [61]. Neat PEI behaves like a typical polymer at low frequencies by drawing a Newtonian plateau independent of frequency. Likewise, it was observed that the complex viscosity did not change significantly for 5 wt% CB contents and shows Newtonian plateau at low frequencies. The Newtonian plateau, however, diminishes when reinforcement content exceeds 10 wt%. These conclusions are consistent with other studies in the literature [64]. Complex viscosity decreased with increasing frequency (shear thinning), and increased reinforcement content resulted in a steeper slope [65].

5.3 Morphological Analysis

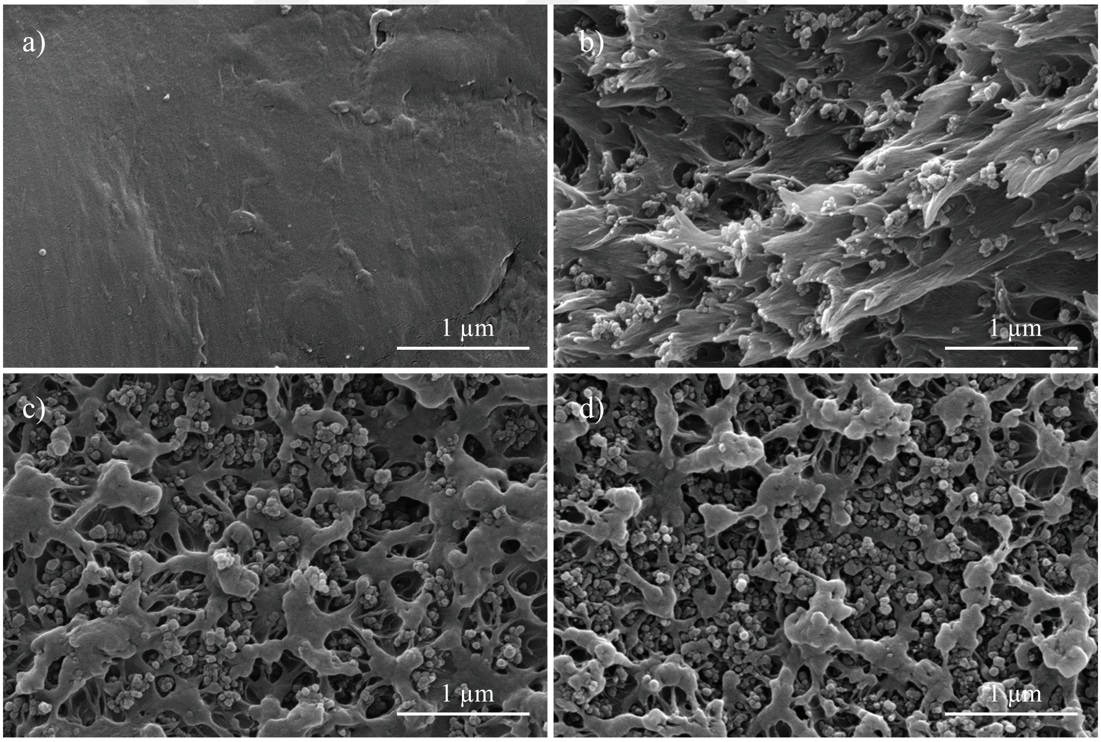

Figure 5.5 : The cross-sectional SEM micrographs of neat PEI, 5, 10, and 20 wt% CB/PEI filaments.

The uniform dispersion of CB particles within the matrix material plays a crucial role in evaluating the mechanical properties of composites, which can vary depending on the amount of reinforcement. Using the SEM technique, the cross-sectional surface morphology of neat PEI and PEI filaments reinforced with 5, 10, and 20% CB were examined. In the SEM images presented in Figure 5.5, CB particles are represented as bright spherical particles and clusters distributed fairly uniformly across all compositions. Due to van der Waals forces, CB tends to form aggregates resembling chains or grape-like clusters ranging from 50 to 500 nm in size [66]. As the proportion of CB increases, an expected increase in CB clusters within the PEI matrix is observed.

5.4 Filament Tensile Test

Tensile tests were conducted on the feedstock filaments to explore the influence of CB reinforcement on their mechanical properties post-production via melt mixing. Using capstan grips, as depicted in Figure 5.6, tensile tests were performed on neat PEI filaments and 5, 10, and 20 wt% CB/PEI composite filaments. The ultimate tensile strength (UTS) of the filaments was measured. Three separate samples were tested for each CB concentration to determine the standard deviation, and the results were reported.

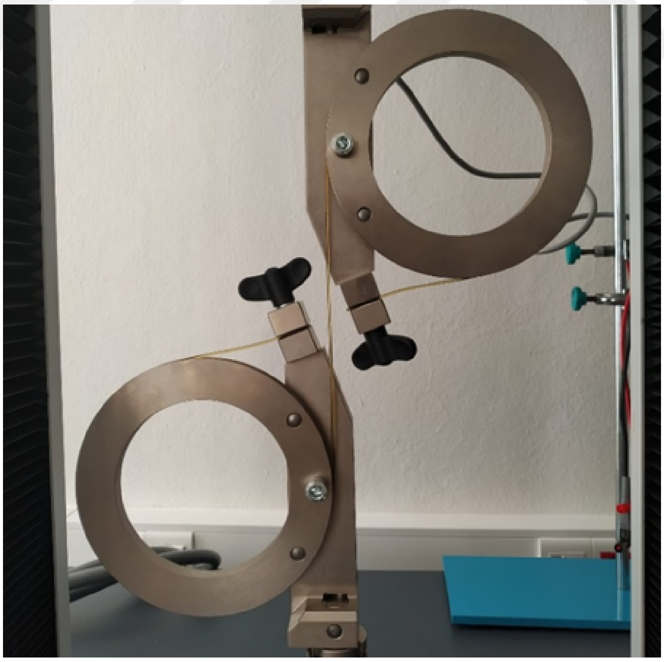

Figure 5.6 : An image from a neat PEI filament tensile test using SHIMADZU AGS-X UTM.

Figure 5.7 presents the stress-strain curves of the feedstock filaments, providing a visual representation of their mechanical behavior. The mean UTS results, along with their standard deviations, were calculated for neat PEI and 5, 10, and 20 wt% CB/PEI as 97.81 ± 0.99, 104.66 ± 1.17, 103.12 ± 0.51, and 81.35 ± 0.82, respectively (see Table 5.2). Notably, the UTS of the neat PEI filament aligns with Sabic's specifications [67], further validating our findings.

The tensile strength of CB-reinforced filaments increased by 7% at 5 wt% CB reinforcement, reaching the highest value. This can be attributed to the homogeneous distribution of the reinforcing material in the matrix and the interaction and adequate wetting between the matrix and the reinforcing material up to 5 wt% CB loading [68]. Adequate wetting of the reinforcement material facilitates load transfer between the matrix and the reinforcement, resulting in increased mechanical strength. It has been shown to decrease slightly when the filler loading increases to 10 wt% and drops abruptly at 20 wt% CB loading. CB particles agglomerate in the matrix as the CB loading increases, creating stress concentration points. As can be seen from the results, it can be said that at 10 wt% loading, CB started to agglomerate and slightly decreased the UTS. At 20 wt% CB loading, the UTS suddenly reduced due to excessive CB in the system [57,69].

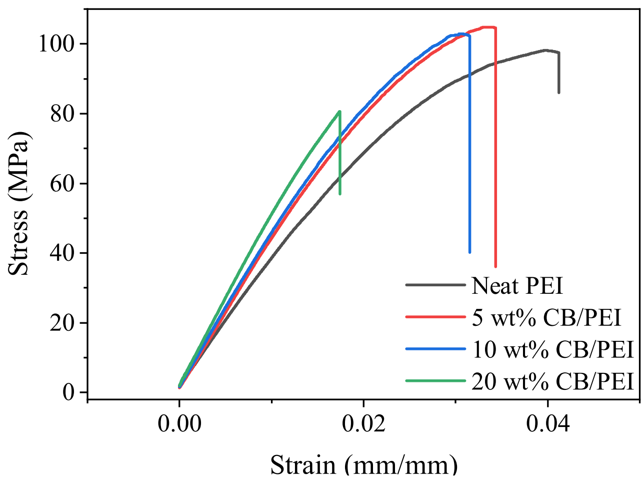

Figure 5.7 : The representative stress-strain curves of neat PEI, 5, 10, and 20 wt% CB/PEI filaments.

CB emerges as a cost-effective reinforcement material for enhancing the mechanical properties of thermoplastic filaments. In our previous research, Yildiz et al. [9]

Table 5.2 : Average UTS results of neat PEI and 5, 10, 20 wt% CB/PEI filaments.

CB concentration (wt%)	UTS (MPa)
Neat	97.81 ± 0.99
5	104.66 ± 1.17
10	103.12 ± 0.51
20	81.35 ± 0.82

reinforced PEI filaments with CNT at concentrations of 1 wt% and 3 wt% to improve their mechanical properties. Interestingly, in this study, we achieved a similar strength value of 104.66 MPa with just 5 wt% CB (see Figure 5.8). This finding underscores the cost-effectiveness of CB as a reinforcement material, offering a comparable level of improvement in the mechanical properties of PEI filaments to CNT. Such findings are particularly relevant for applications that balance performance and cost efficiency.

The reinforcement strategy to enhance the mechanical properties of 3D printing filaments has some drawbacks. When the reinforcements in the polymer matrix exceed a specific concentration, the composite filaments cross the rheological percolation threshold, leading to changes in their microstructure. This results in a significant increase in the viscosity of the composites, thereby reducing the printability of the filaments [57]. The previous section thoroughly examined the rheological properties of CB-reinforced filaments. Upon analysis, it was found that the rheological percolation threshold of CB/PEI composite filaments was at a CB concentration of about 10 wt% [14]. This finding indicates that the viscosity remains below the rheological percolation threshold at 5 wt% CB concentration, allowing easy printing at low viscosity values during FFF. Furthermore, the highest mechanical strength value was observed at 5 wt% CB loading. Therefore, 5 wt% CB reinforcement offers the best result by ensuring easy printability and the highest mechanical strength value. This finding underscores the importance of considering both rheological and mechanical aspects when determining the optimal CB concentration for improved performance in the FFF process, thereby making our research highly relevant to practical 3D printing applications.

However, although CB reinforcement improves the mechanical properties, it compromises the multifunctional properties of the filaments. The electrical conductivity of CNT-reinforced PEI is significantly higher than that of their

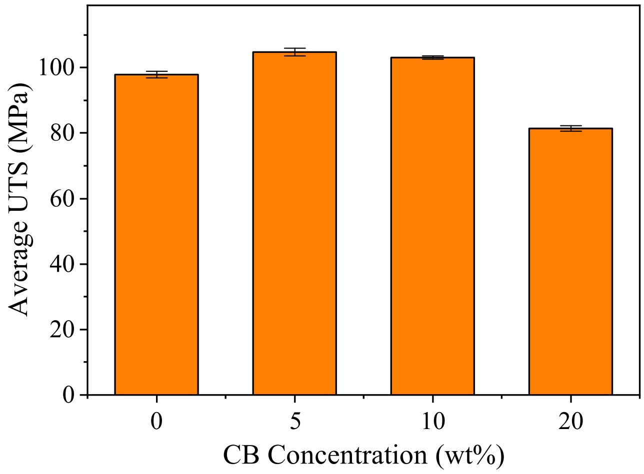

Figure 5.8 : The average UTS results of neat PEI, 5, 10, and 20 wt% CB/PEI filaments with their standard deviations.

CB-reinforced counterparts. Based on the previous study [9], the electrical percolation threshold of CNT/PEI composites was well below the concentration of 1 wt% CNT. In contrast, no significant electrical conductivity was measured for CB reinforcement (<$10^{-}5$ S/cm). This difference may be due to the 1-dimensional (1-D) nature and high aspect ratio of CNTs, which form a conductive network pathway that can facilitate electron conduction even at low concentrations within the polymer matrix [70]. In the case of 0-dimensional (0-D) CB, much higher amounts of filler are required to reach the electrical percolation threshold than CNTs.

5.5 Creep Analysis

5.5.1 Creep test under double cantilever fixture

The creep strain curves of 3D-printed specimens produced with neat PEI, 5 and 10 wt% CB/PEI were shown in Figure 5.9. A primary creep stage was observed in the curve at each temperature following the instantaneous strain, an elastic deformation. In this stage, the creep strain increased with time at a decreasing rate. Subsequently, the specimens transitioned to the secondary creep region with a constant creep rate [15]. The final creep stage, the tertiary creep phase, which ends in rupture, was not observed in any specimens due to the short test duration for high-strength thermoplastics such as PEI. Moreover, larger instantaneous strain and steeper creep strain curves were observed at higher temperatures, indicating a higher creep rate at higher temperatures.

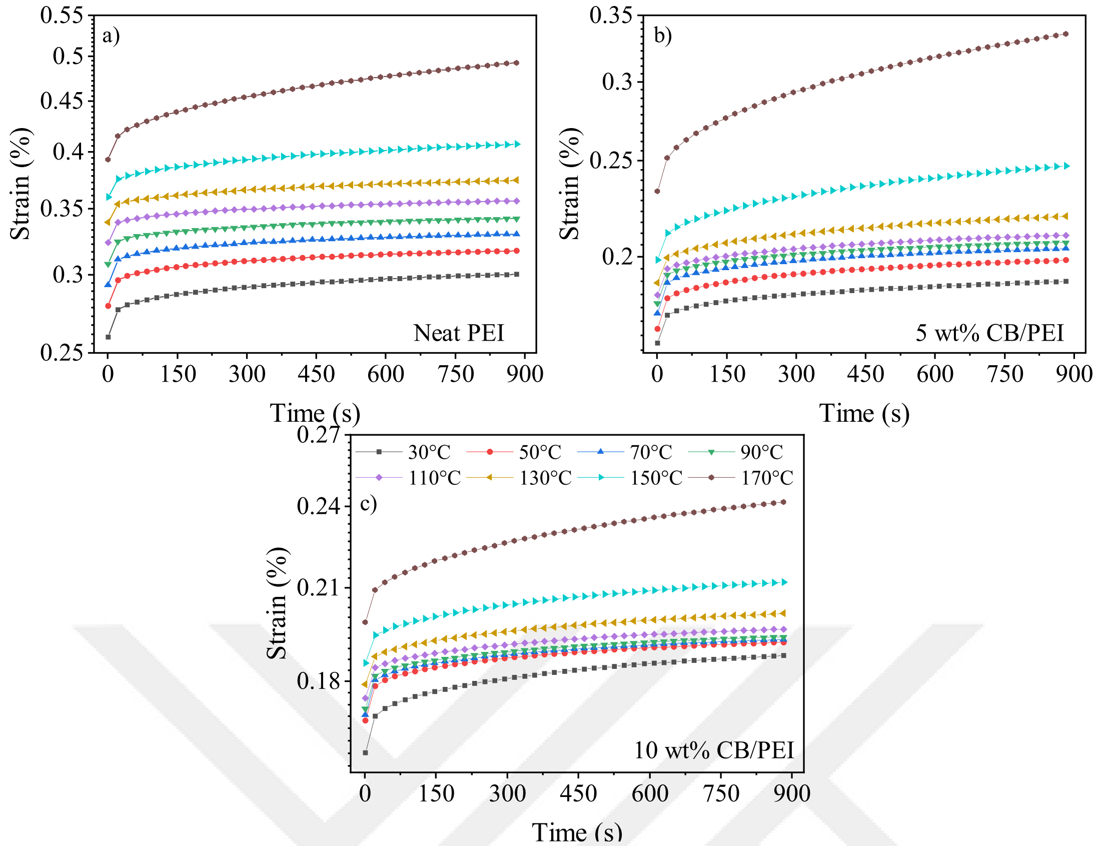

Figure 5.9 : Creep strain curves of 3D-printed neat PEI, 5 and 10 wt%CB/PEI specimens at the range of 30-170 °C.

For instance, neat PEI exhibited instantaneous strains of 0.25955% and 0.39251% at 30 °C and 170 °C, respectively. Therefore, it can be concluded that when the polymer matrix is exposed to high temperatures, the chain mobility and entanglement increase, thus reducing the composite's stiffness and leading to deformation.

To better analyze the effects of CB reinforcement, the creep strain curves of the samples at the limit temperatures of characterization, 30 °C and 170 °C, were plotted in Figure 5.10 as a function of time. The results revealed that as the reinforcement concentration increases, the creep strain of the composites decreases significantly in each isotherm. This phenomenon can be attributed to CB particles effectively dispersed among the polymer chains, hindering chain mobility and reducing strain at higher CB concentrations [71]. Furthermore, the creep resistance was observed to be enhanced with higher CB content, particularly at elevated temperatures. This observation suggests that CB reinforcement builds resistance to deformation even

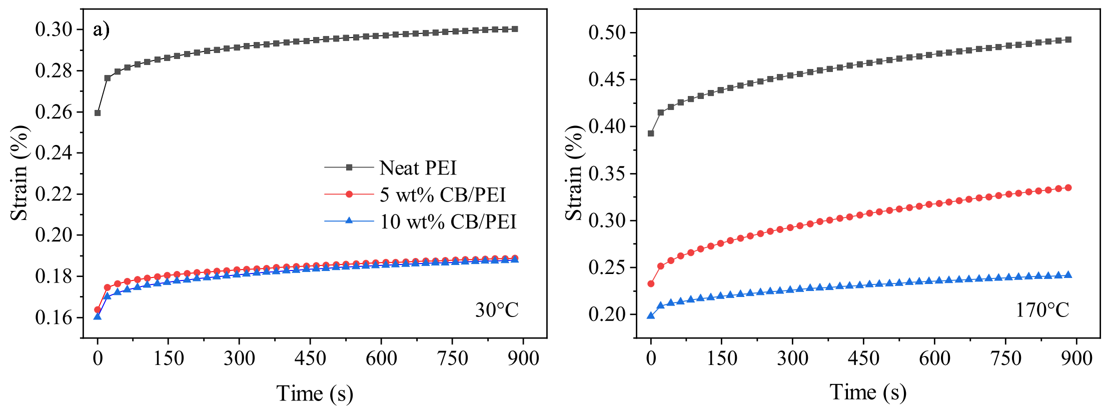

Figure 5.10 : Creep strain curves of all specimens at a) 30 °C and b) 170 °C .

under high-temperature conditions. This behavior may be attributed to forming a thermally conductive network by CB particles, facilitating heat dissipation within the structure and mitigating creep deformation.

5.5.2 Creep test under three-point bending fixture

Creep tests of all specimens were carried out using the second test protocol (using 3 point bending fixture) described in detail in section 4.4.5 . Hot-pressed neat PEI and 3D-printed neat PEI and CB-reinforced composites at elevated temperatures were shown in Figure 5.11. The average value of three different samples was used to plot each creep curve. The creep curves for all CB concentration specimens and the hot-pressed specimen showed a similar pattern: An instantaneous strain is observed when the load is first applied to the specimen. When the specimen is applied to the load for the first time, it undergoes an elastic deformation associated with stretching the polymer chains and the bonds between the molecules. Following the instantaneous strain, a primary creep phase was observed in the specimens. Time-dependent increases at a decreasing rate characterized this phase of creep deformation. Then, the specimens transitioned to the secondary creep phase with a constant creep rate [15]. Especially for high-strength thermoplastics such as PEI, the tertiary creep phase, defined as permanent viscous deformation resulting in specimen rupture, could not be observed because of the short testing duration.

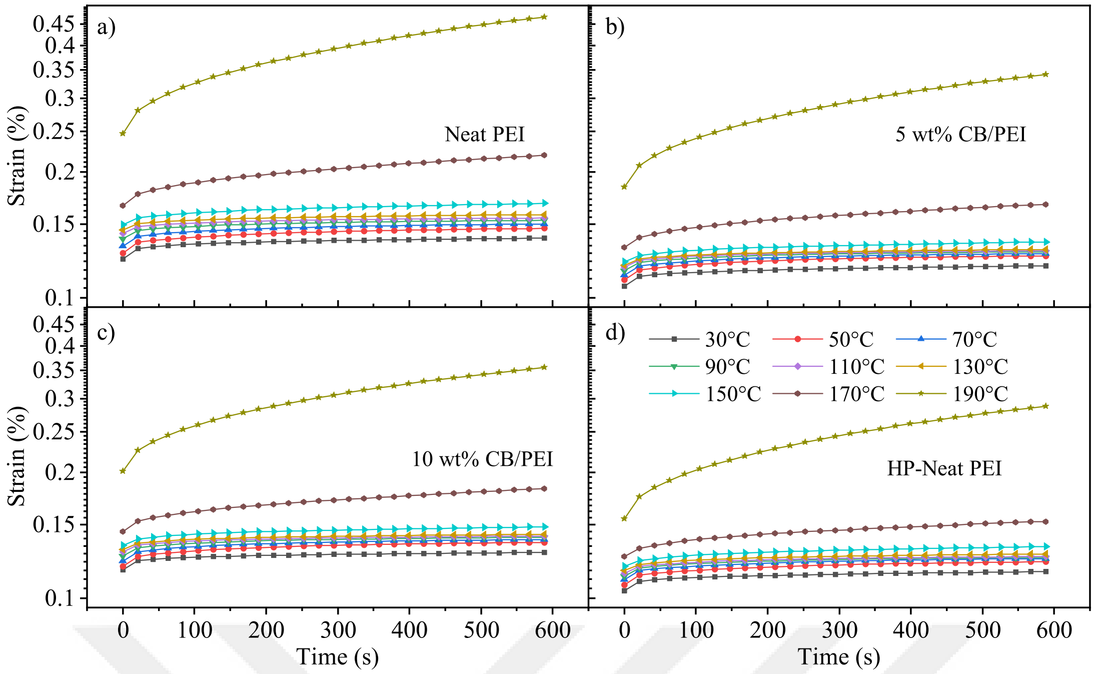

Figure 5.11 : Time-dependent creep strain curves of 3D printed a) neat PEI, b) 5 wt% CB/PEI, c) 10 wt% CB/PEI, and d) hot pressed neat PEI specimens in the range 30-190 °C.

Furthermore, when these curves are examined, it becomes evident that the samples exposed to higher temperatures exhibit larger instantaneous strains and steeper slopes in the creep strain curves. For example, as given in Table 5.3, the instantaneous strain of neat PEI was measured as 0.124±0.012% and 0.247±0.033% at 30 °C and 190 °C, respectively. These findings suggest that exposing the polymer matrix to elevated temperatures enhances chain mobility, subsequently reducing the stiffness of the composites and promoting deformation tendencies.

Table 5.3 : Instantaneous creep strain values of all specimens in the range 30-190 °C.

Temp. (°C)	Instantaneous Strain (%)			
	Neat PEI	5 wt% CB/PEI	10 wt% CB/PEI	HP-Neat PEI
30	0.124±0.012	0.107±0.004	0.117±0.010	0.104±0.006
50	0.128±0.012	0.110±0.006	0.119±0.010	0.107±0.008
70	0.133±0.014	0.113±0.006	0.122±0.011	0.111±0.009
90	0.138±0.016	0.116±0.007	0.126±0.012	0.113±0.010
110	0.142±0.018	0.118±0.007	0.129±0.013	0.115±0.010
130	0.145±0.019	0.120±0.008	0.131±0.014	0.117±0.010
150	0.149±0.020	0.122±0.009	0.134±0.015	0.119±0.010
170	0.166±0.023	0.132±0.012	0.144±0.018	0.126±0.009
190	0.247±0.033	0.184±0.023	0.201±0.029	0.155±0.009

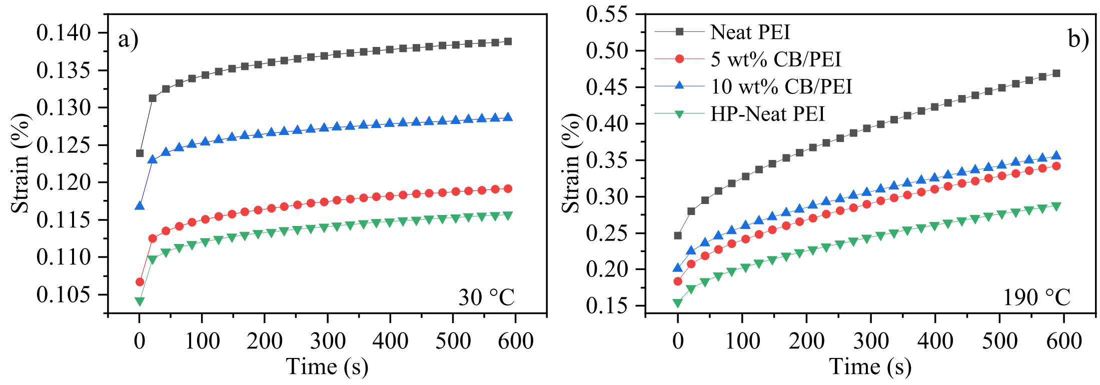

Figure 5.12 : Creep strain curves of all specimens at a) 30 °C and b) 190 °C.

For a more comprehensive analysis of the effect of CB reinforcement, the creep strain curves of the specimens at 30 °C and 190 °C were plotted over time in Figure 5.12. The results highlight a significant reduction in creep deformation for the creep curve at each temperature in the presence of CB reinforcement. The creep strain of 5 wt% and 10 wt% CB reinforcement decreased by 14% and 7%, respectively, compared to the 3D printed neat PEI specimens at 30 °C. This finding can be attributed to the effective dispersion of CB particles between polymer chains, which inhibits chain mobility and stiffness of the composite, resulting in lower deformation at higher CB concentrations [71]. Moreover, this increase is more pronounced at higher temperatures. At 190 °C, specimens reinforced with 5 wt% and 10 wt% CB showed a 26% and 19% reduction in creep strain.

Examination of the creep curves at both 30 °C and 190 °C revealed that the hot-pressed sample exhibits the most minor creep deformation. This is an expected result due to the inherently porous nature of 3D printing, resulting in lower mechanical strength values than conventional manufacturing methods. The results showed that adding 5 wt% CB reinforcement to the 3D-printed PEI gave the closest results to the hot-pressed sample. This result is noteworthy as it implies an improvement in creep behavior, consistent with the findings from the filament tensile tests. The 5 wt% reinforcement shows a compensating effect by reducing the negative impact of 3D printing on the mechanical properties and optimally improves the creep resistance.

To more clearly understand the effect of CB concentration in the PEI matrix from a reproducibility point of view, the maximum creep strain of the specimens at each temperature is presented in Figure 5.13a, along with the corresponding standard deviations. The main point to be noted here is the amount of standard deviations. The deviation values in the data from the three samples produced for each different concentration can provide information to show the repeatability in production with the respective filament. Although the three samples are not a large enough statistical cluster, the observed values of the deviations show that, as in creep, 5 wt% CB/PEI samples and the hot-pressed neat PEI samples are similar. These specimens, produced by two different methods and with two different raw material forms (filament and pellet), can be produced with a similar consistency, and specimens of the same raw material can exhibit very similar mechanical values.

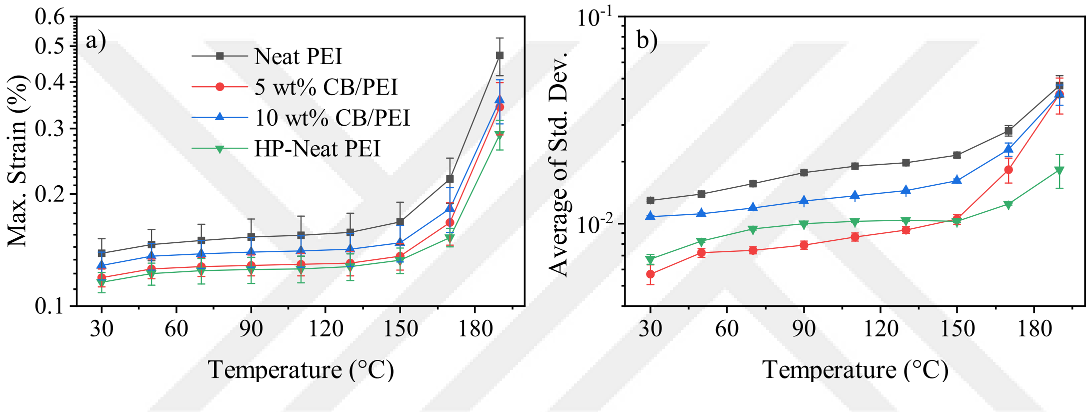

Figure 5.13 : a) The average maximum strain values and standard deviations of the specimens at each temperature, b) the average and deviation values of the standard deviations of all strain values.

To extend this discussion to all measured values of maximum creep strain, one can look at the average values of the standard deviations, although this is not a common approach. Figure 5.13b shows the mean values of the standard deviations of the strain values obtained versus time at each temperature for all specimens. The deviation values of these averages have also been added to the graph. It is seen that as the temperature increases, the deviation values of all specimens also increase. The specimens with the lowest deviation values were the 5 wt% CB/PEI specimens, which exhibited very similar values to the hot-pressed neat PEI specimens produced by the conventional method. In this context, it can be said that doping PEI thermoplastic with 5 wt% CB positively affected the additive manufacturing process and overcame deficiencies such as decreased mechanical values and reproducibility compared to the conventional production method.

5.6 Creep Modeling

5.6.1 Modeling of creep results under double cantilever fixture

Modeling the creep behavior of materials using mathematical functions is essential from an engineering standpoint, as it allows for predicting the material's performance in real-world applications. Experimental data of creep strain as a function of time for 3D-printed neat PEI, 5 wt% CB/PEI, and 10 wt% CB/PEI, along with their fitting curves obtained using the Burgers and Findley model functions, were presented in Figure 5.14. Although the Burgers and Findley models exhibit good agreement with the experimental data at all temperatures, only the modeling results at 30 °C are depicted for clarity. The parameter values of the Burgers and Findley models obtained from curve fitting for all samples are provided in Table A.1 and Table A.2, respectively. Additionally, the goodness of fit is evaluated using the reduced (Red.) χ^2 and adjusted (Adj.) R^2 values, which were also reported in the tables.

Examining the curve fitting results of the Burgers and Findley models, it is observed that the Burgers model, represented by the red line, did not successfully estimate the instantaneous strain and the primary creep region. Conversely, in the last minutes of the creep test, the Burgers model tends to overestimate the creep strain. This outcome is expected because the Burgers model includes a Maxwell dashpot to simulate the viscous creep phase (tertiary creep region). However, since the duration of the creep test conducted may not be long enough to traverse through the viscous deformation region, this phase is not observed, potentially leading to overestimation by the model. Upon examining the Red. χ^2 and Adj. R^2 values in Table A.1, which is about the suitability of the Burgers model, overall, the Burgers model adequately captures the creep behavior of PEI.

On the other hand, as seen in Table A.1, the Maxwell unit's elastic modulus E_M corresponds to the samples' instantaneous elastic strain. Therefore, as the polymer chains became more mobile and more prone to deformation under high temperatures,

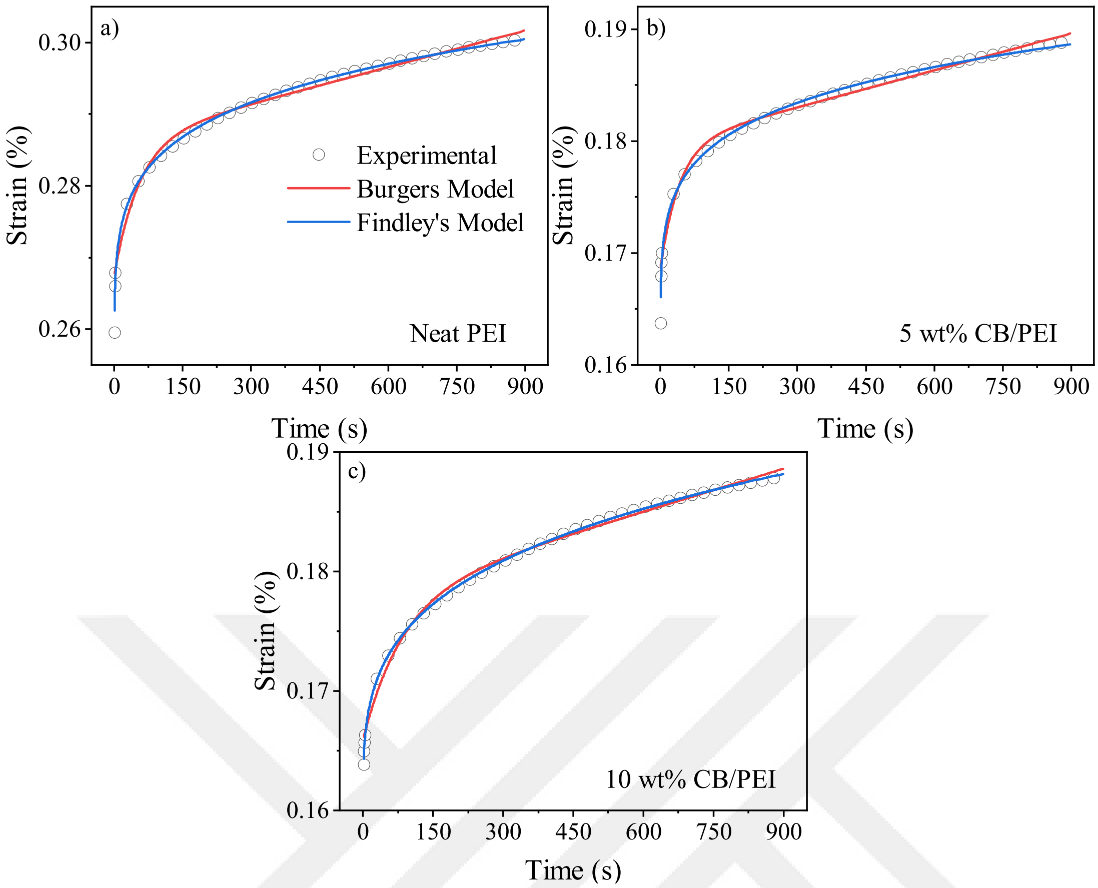

Figure 5.14 : Curve fitting results were obtained using Burgers and Findley's model for the strain at 30 °C of 3D-printed a) neat PEI, b) 5 wt% CB/PEI, and c) 10 wt% CB/PEI specimens.

the E_M decreased with increasing temperature, consistent with the instantaneous strain experiments. This behavior results in lower modulus and higher strain results. In addition, all temperatures showed an increase in E_M with increasing concentration of CB reinforcement because the CB particles restrict the movement of polymer chains and contribute more stiffness to the specimens.

Similar to the Burgers model, the Findley function, depicted by the blue line, effectively captured the creep behavior of PEI. Furthermore, in contrast to the Burgers model, the Findley function better simulated both the primary creep region and the final stage of the creep test. This conclusion is supported by the smaller Red. χ^2 and Adj. R^2 values observed in Table A.2. As expected, the parameter ε_0 decreased with the concentration of CB reinforcement at all temperatures and increased with temperature. Parameter A exhibited an increasing trend up to a peak value between 50-70 °C, followed by a decreasing trend. Additionally, it decreased with the concentration of CB reinforcement in each isotherm. Conversely, the exponent n decreased to a minimum value between 50-70 °C and then increased with temperature. Moreover, it increased with CB content in almost all isotherms.

5.6.2 Modeling of creep results under three-point bending fixture

Experimental creep strain data for 3D-printed neat PEI, 5 wt% CB/PEI, 10 wt% CB/PEI, and HP-Neat PEI at 30 °C as a function of time were modeled using Burgers, Findley, and Generalized Kelvin functions. Figure 5.15 shows these curve-fitting results. Based on the Red. χ^2 and Adj. R^2 results of the Burgers, Findley, and Generalized Kelvin model shown in Tables A.3, A.4, and A.5 respectively, it can be concluded that all functions give satisfactory results with the experimental results.

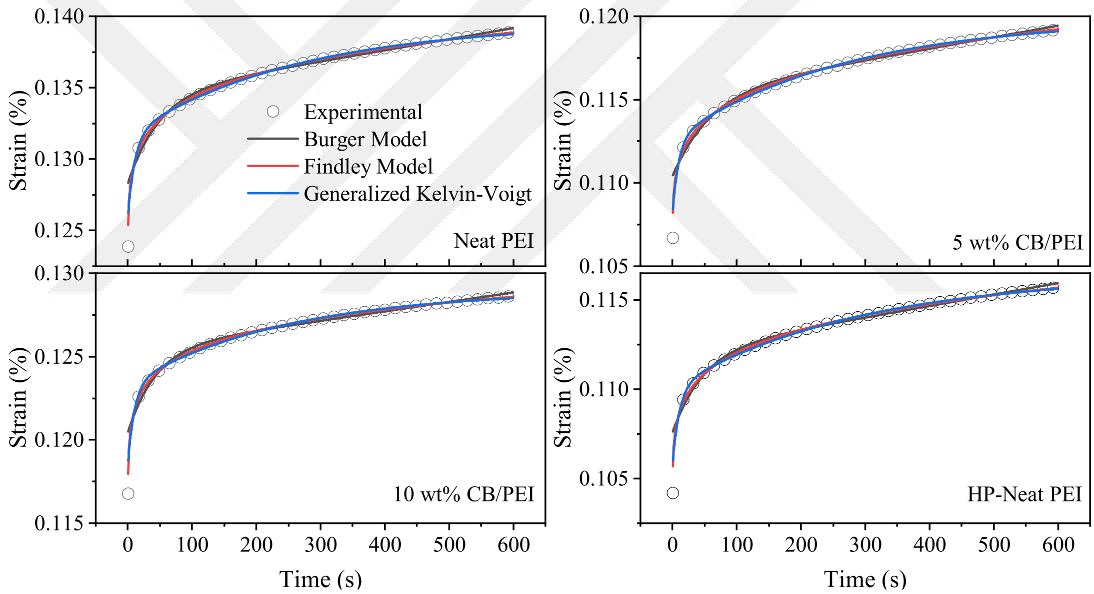

Figure 5.15 : Simulation results of strain curves of 3D-printed a) Neat PEI, b) 5 CB/PEI, c) 10 CB/PEI, and d) HP-Neat PEI samples at 30°C using three different models.

The Burgers model, represented by the black solid line in the graphs, exhibited a slight deviation during the simulation of the primary creep stage in all specimens. Table A.3 tabulates the four Burgers model parameters (E_M, E_K, η_M, and η_K) used to fit Equation 3.17 to the experimental data. The Maxwell unit's elastic modulus, denoted as E_M, reflects the elastic part of the specimens. Therefore, E_M decreased with increasing temperature, inversely proportional to the experimental instantaneous strain results. This phenomenon can be attributed to the increased mobility of polymer chains at high temperatures, which makes them more susceptible to deformation. Furthermore, the observed trend revealed that the E_M increased proportionally to the CB reinforcement concentration at all temperatures. This is attributed to the CB particles, which impart greater stiffness to the specimens by restricting the movement of the polymer chains. In contrast, the Burgers model encountered problems accurately capturing the instantaneous strain and the onset of creep behavior for all specimens. A closer examination of the final stage of the creep curves revealed that the model slightly overestimated the creep behavior. This discrepancy is due to the Kelvin dashpot in the Burgers model, which allows it to simulate viscous deformation. However, the duration of the creep test applied in this research is insufficient to observe the viscous phase of creep fully. Therefore, the Burgers model overestimates the results when simulating the final phase of the creep curves.

On the other hand, the creep behavior was well represented by the empirical Findley power law, indicated by Red. χ^2 values smaller than those obtained using the Burgers model at all temperatures. As expected, the ε_0 value increased with increasing temperature and decreased in parallel with the CB reinforcement concentration at each temperature. The Parameter A showed an increasing trend, peaking between 50 and 90 °C and then decreasing. Moreover, A showed a decrease in response to the CB supplement concentration in each isotherm. On the other hand, as the temperature increased, the n exponent decreased to a minimum value between 50 and 90 °C and then started to increase. Moreover, n was shown to increase with CB content in almost all isotherms.

5.6.3 TTSP

To obtain a master curve according to the TTSP, two different approaches were tried: model-based and manual shifting. In the first method, the TTS R library mentioned in Section 2.1.2 was used to derive master curves based on the WLF equation (Eq. 3.20) and the Arrhenius equation (Eq. 3.21). The reference temperature was fixed at 30 °C, and the algorithm was expected to identify the curves. However, due to the complex

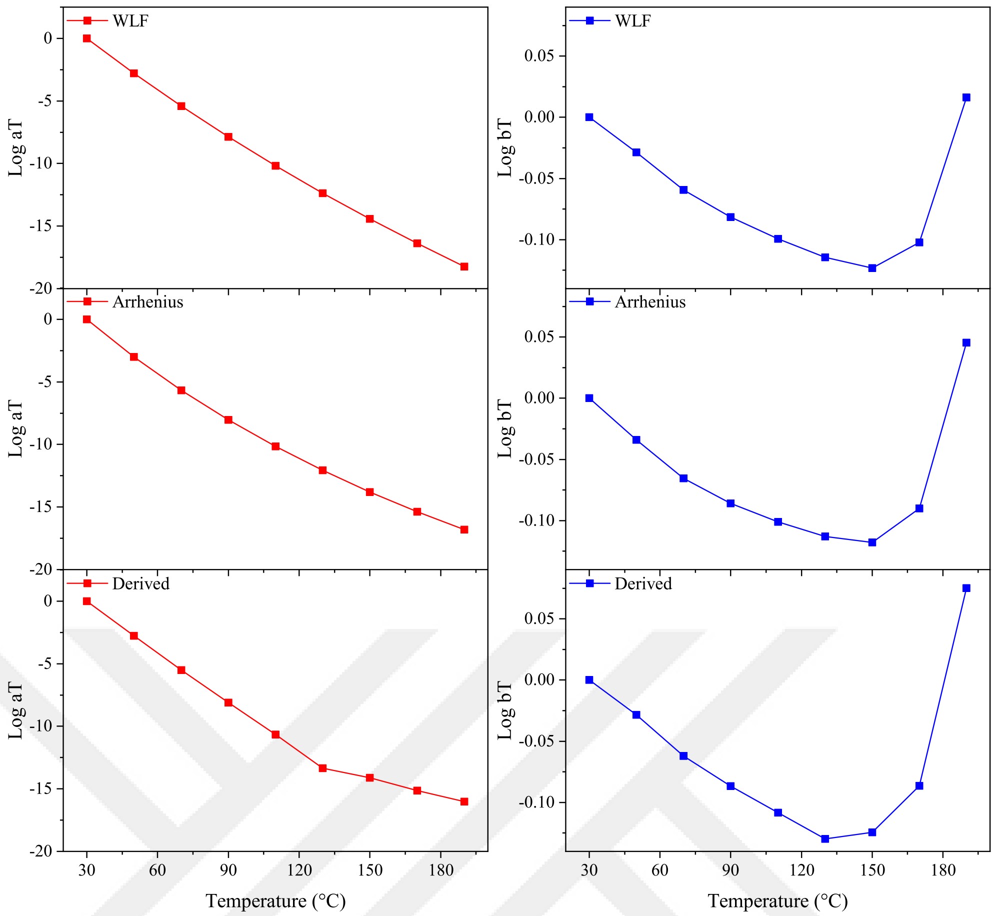

Figure 5.16 : Obtained shift factors using TTS R library based on (a) WLF, (b) Arrhenius, (c) MNAT methods.

thermo-rheological nature of PEI, neither equation provided reasonable shift factors to create a single, coherent master curve. This challenge with PEI has been noted in various sources in the literature [12,17].

As another model, the MNAT approach developed by Naya et al., available within the TTS R library, was employed. The shift factors obtained using WLF, Arrhenius and MNAT approach were given in Figure 5.16. Obtained mastercurves using these shift factors, also, plotted in Figure 5.17. As seen in the graph MNAT approach gives better curve fit. Figure 5.18 represents the creep master curves at 30 °C for neat PEI, hot-pressed PEI, and 5 wt%, 10 wt% CB/PEI obtained using this method by horizontally and vertically shifting the curves. This method, adaptable to any temperature to obtain creep master curves, selected 30 °C as the reference temperature

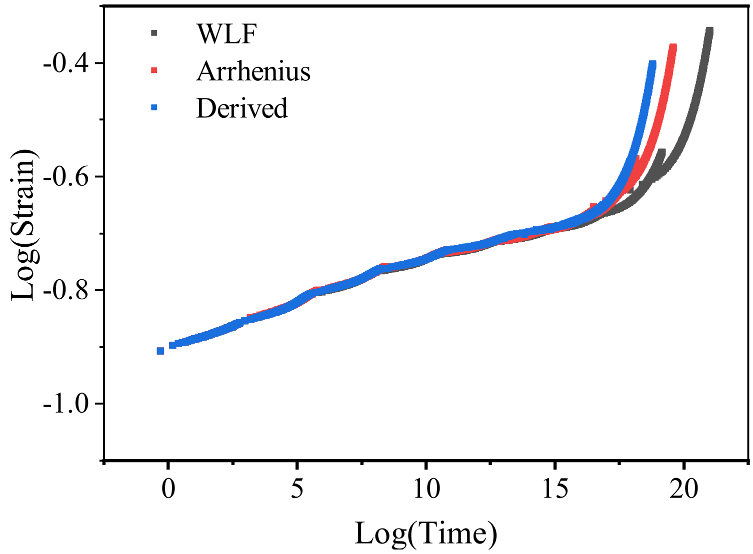

Figure 5.17 : The mastercurves using obtained shift factors.

to determine the long-term creep behavior of specimens intended for use at room temperature.

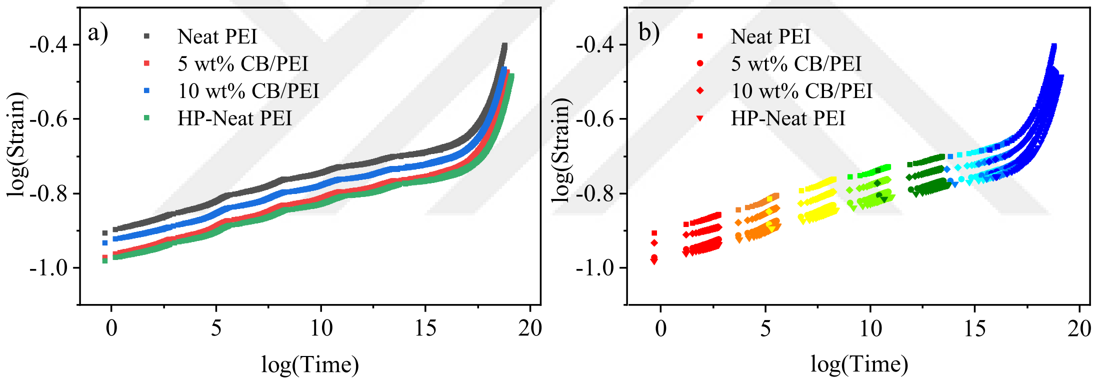

Figure 5.18 : Creep master curves of 3D printed neat PEI, 5 wt% CB/PEI, 10 wt% CB/PEI and HP-Neat PEI. a) Using all data b) Generated creep master curves with data points reduced to one at 15.

As depicted in Figure 5.18a, the derived creep master curves reach up to 10^{18} seconds on the time axis, in contrast to the more commonly reported values around 10^{9} seconds in the literature [10,12,17], thus raising questions about their validity. The MNAT procedure applied during TTS calculations uses the derivatives of the creep curves to determine the shift factors [52]. Analyzing the creep curves obtained at lower temperatures reveals that PEI, due to its high mechanical strength, exhibits nearly linear behavior. This indicates that the algorithm tends to concatenate the creep curves across different temperatures. This effect is more clearly observed in Figure 5.18b, where the color map of the creep master curves, plotted with fewer data points, demonstrates this behavior more explicitly.

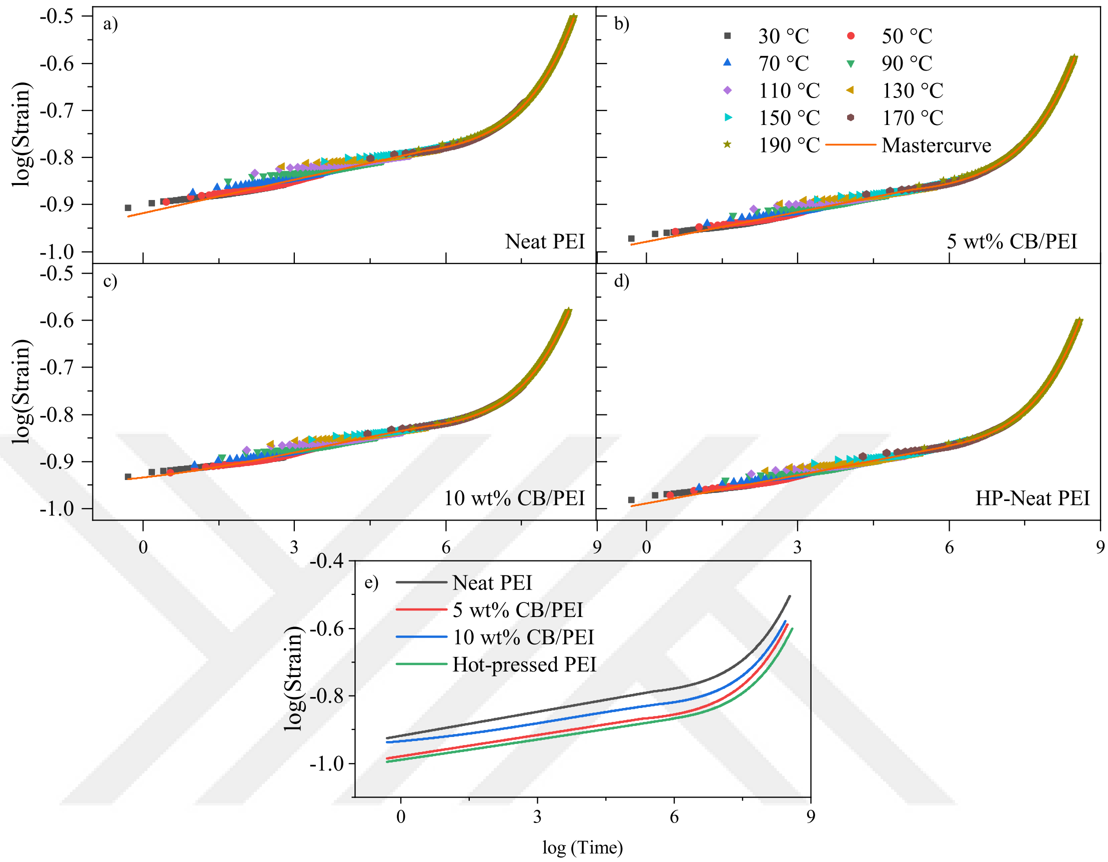

Figure 5.19 : Creep master curves of 3D printed neat PEI, 5 wt% CB/PEI, 10 wt% CB/PEI and HP-Neat PEI. a) Using all data b) Generated creep master curves with data points reduced to one at 15.

Due to the inability to achieve reasonable results with model-based methods, a manual shifting approach was implemented as an alternative. A Python script was developed in Jupyter Notebook to manually adjust all temperature curves both vertically and horizontally. Figure 5.19 displays the manually shifted creep master curves for neat PEI, hot-pressed PEI, and 5 wt%, 10 wt% CB/PEI. Various functions were attempted to fit these curves, and the fitting results are shown in Figure 5.19e . Despite trying different functions to model the creep master curves, none provided an adequate simulation of the entire curve. Upon analyzing the creep master curves, it was noted that the creep strain changes linearly up to approximately 10^6 seconds, after which a sigmoidal change is observed. Consequently, separate curve fits were applied using linear and sigmoidal functions (Figure 5.19e).

Using both methods, the resulting creep master curves align well with the short-term experimental creep data. The hot-pressed neat PEI specimen demonstrated the greatest resistance to creep, while the 5 wt% CB-reinforced PEI specimen exhibited a creep behavior that closely paralleled that of the hot-pressed sample.

5.7 Key Outcomes and Further Discussion

The impact of CB reinforcement on the mechanical properties of PEI composites produced through FFF was analyzed in details, with a specific emphasis on their creep characteristics. Several challenges and limitations inherent to additive manufacturing were identified during this thesis study. One major challenge was that reinforcing CB to the polymer matrix increased its viscosity and aked changes in its flow characteristics, limiting the CB content to a maximum of 20 wt%. Even at this threshold, the filaments exhibited high brittleness, rendering them unsuitable for the FFF process. Another crucial factor influencing the mechanical properties of the samples is the infill ratio of the 3D-printed specimens. To replicate the qualities of conventionally manufactured parts and achieve optimal performance, a 100% infill ratio was selected for this study.

Although the effect of printing temperature on the mechanical properties was not directly investigated, temperatures were chosen based on prior experience to ensure optimal results [9]. In addition, the variability and anisotropy inherent in FFF-produced samples posed another limitation. In the dual cantilever tests, creep test specimens were manufactured and tested as single specimens per concentration, leading to inconsistencies. For instance, the creep performance of specimens with 10 wt% CB was the best, which was contrary to the tensile test results. To mitigate these issues, a different approach was tried by using a 3-point bending fixture instead of a dual cantilever fixture. This fixture was selected for its simplicity and ease of setup, particularly since more complex properties like the shear modulus were not assessed. Importantly, three tests were conducted for each type of specimen, allowing for evaluations based on the mean and standard deviation, thus improving the reliability of the data. Despite the limited number of specimens tested due to the lengthy duration of each test and budget constraints, this method provided more robust and reliable results compared to the single-specimen approach previously used.

The key findings of this study are encapsulated in Table **??**.Furthermore, Table 5.5 presented a comparison of the mechanical properties observed in this study with those reported in similar studies from the literature. This comparative analysis underscores the relevance and significance of our findings within the broader context of existing research.

Table 5.4 : Main outcomes and summary of the this study.

Property	Outcomes
Thermal	No significant change in thermal decomposition with CB.
Rheological	Rheologically percolated around 10 wt% CB Printing difficulties due to high viscosity.
Tensile	7% Enhancement in UTS with 5 wt% CB. Too brittle for printing at 20 wt% CB
Creep (strain)	14% reduced at 30 °C with 5 wt% CB. 19% reduced at 150 °C with 5 wt% CB.
Creep Modeling	Findley model gave the best curve-fit results. Burgers model overestimates the final phase of the creep curves. Burgers model did not capture the instantaneous strain effectively. The terms of Kelvin-Voigt model were inconsistent.

This investigation revealed a 7% increase in UTS with the incorporation of 5 wt% CB into PEI filaments. This enhancement is consistent with findings from other studies (Table 5.5), demonstrating the efficacy of CB in improving tensile properties. Moreover, it establishes CB as a cost-effective yet efficient reinforcement material compared to other carbon-based reinforcements. However, the study also noted increased brittleness at higher CB concentrations (10 wt% and 20 wt%), which poses a significant challenge for practical applications.

Furthermore, the addition of 5 wt% CB improved the creep resistance of PEI composites. As depicted in Table 5.5, various reinforcing agents have been shown to enhance the creep behavior of PEI, though literature on this topic is limited. While

CB has been reported to improve the creep behavior of polymers in numerous studies, no specific research addressing the creep behavior of PEI with CB reinforcement was identified. Consequently, a direct quantitative comparison with this study is not possible. It is also important to note that none of the existing studies involve samples produced using FFF.

Table 5.5 : Comparing the outputs of this study (marked by *) with the findings reported in the literature.

Property	Polymer	Reinforcement	Result
UTS	PEI (Ultem 1010)*	5 wt% CB	7% Enhancement
	PEI (Ultem 1010) [9]	3 wt% CNT	7% Enhancement
	PEI (Ultem 1000P) [72]	5 wt% CNT	6% Enhancement
	PEI (Ultem 1000) [73]	5 wt% SCF	7% Enhancement
	PEI (Ultem AUT 100) [68]	2 wt% MWCNT-COOH	7% Enhancement
	PEI (Ultem R00H) [74]	10 wt% CF (2000 μm)	7% Enhancement
Creep	PEI (Ultem 1010)*	5 wt% CB	Creep strain decreased by ca. 14%
	PEI (Ultem 1000) [73]	5 wt% SCF	Creep strain decreased by ca. 30%
	PEI (Ultem 1000) [13]	10 wt% CF	CF reduced the growth rate of cyclic creep
	Polyethylene [75]	1 wt% CB	Creep resistance improved by ca. 35%
	SBR and NBR rubber [76]	20-70 wt% CB	More CB improved relax. and reduced creep
	Epoxy carbon fiber [77]	4 wt% nano CB	Creep strain improved by ca. 19%
	Poly(methyl methacrylate) [78]	2-5 vol%CB	Higher CB enhanced creep recovery.

In future studies, efforts will be directed towards implementing various methods to further enhance the mechanical performance of samples produced via FFF. Several techniques in the literature aim to improve the interlayer adhesion of FFF parts. For example, Tofangchi et al. [79] increased polymer chain reptation at the interface by utilizing ultrasonic vibration, which relaxes the polymer chains. Another innovative approach by Stano et al. [80,81] involves ironing, where mechanical pressure is applied to the printed layers with the nozzle tip. This process enhances chain diffusion between layers and reduces porosity cost-effectively without needing additional mechanisms.

By implementing these methodologies, future research aims to significantly improve the mechanical properties of high-performance thermoplastic composites. Integrating these advanced techniques is expected to address the current limitations of FFF, making it a more viable option for applications that demand high-performance materials.

6. CONCLUSION

In this thesis, the mechanical properties of CB reinforced PEI composite materials produced using the FFF technology were investigated. FFF technology offers advantages such as low cost, ease of use, and minimal waste production. However, a significant drawback of FFF is the lower mechanical strength of the produced parts compared to those manufactured using conventional methods. This study aimed to address this disadvantage by reinforcing PEI material with CB.

Initially, composite filaments containing different ratios of CB (5%, 10%, and 20% by weight) were prepared using a co-rotating twin-screw extruder, and creep test samples were produced from these filaments. During the characterization phase, thermal, rheological, morphological, and mechanical properties were examined. It was found that CB reinforcement did not affect the thermal stability of PEI filaments but increased the complex viscosity and tensile strength at certain ratios. The highest tensile strength was obtained with 5% CB reinforcement, while decreases in tensile strength were observed at 10% and 20% CB concentrations.

Creep tests revealed that CB reinforcement significantly enhanced the mechanical performance of PEI samples. The 5% CB/PEI samples exhibited creep behavior similar to conventionally produced pure PEI samples. This finding indicated that the mechanical strength lost in FFF-produced samples could be regained with CB reinforcement.

The experimental creep data were mathematically modeled using Burgers, Findley power law, and generalized Kelvin-Voigt models. The Findley power law model was found to be more consistent with the experimental results. Additionally, TTSP curves were created to analyze the thermal and mechanical behaviors of PEI in more detail. The TTSP master curves obtained using the MNAT procedure and manual shifting methods provided more reasonable results compared to other methods in the literature.

In conclusion, this thesis demonstrated that the mechanical properties of high-performance composite materials could be improved by producing them with FFF technology, thus increasing their potential use in advanced technology applications. This study, focusing on optimizing the mechanical strength and creep resistance of PEI and CB-reinforced composites, makes a significant contribution to the wider industrial application of FFF-based 3D printers.

REFERENCES

[1] **Gibson, I.**, **Rosen, D.W.**, **Stucker, B.**, **Khorasani, M.**, **Rosen, D.**, **Stucker, B. and Khorasani, M.** (2021). *Additive manufacturing technologies*, volume 17, Springer.

[2] **Han, P.**, **Tofangchi, A.**, **Deshpande, A.**, **Zhang, S. and Hsu, K.** (2019). An approach to improve interface healing in FFF-3D printed Ultem 1010 using laser pre-deposition heating, *Procedia Manufacturing*, *34*, 672–677.

[3] **Liaw, C.Y.**, **Tolbert, J.W.**, **Chow, L.W. and Guvendiren, M.** (2021). Interlayer bonding strength of 3D printed PEEK specimens, *Soft matter*, *17*(18), 4775–4789.

[4] **Lay, M.**, **Thajudin, N.L.N.**, **Hamid, Z.A.A.**, **Rusli, A.**, **Abdullah, M.K. and Shuib, R.K.** (2019). Comparison of physical and mechanical properties of PLA, ABS and nylon 6 fabricated using fused deposition modeling and injection molding, *Composites Part B: Engineering*, *176*, 107341.

[5] **Ding, S.**, **Zou, B.**, **Wang, P. and Ding, H.** (2019). Effects of nozzle temperature and building orientation on mechanical properties and microstructure of PEEK and PEI printed by 3D-FDM, *Polymer Testing*, *78*, 105948.

[6] **Kaynan, O.**, **Yıldız, A.**, **Bozkurt, Y.E.**, **Yenigun, E.O. and Cebeci, H.** (2020). Electrically conductive high-performance thermoplastic filaments for fused filament fabrication, *Composite Structures*, *237*, 111930.

[7] **Wu, H.**, **Sulkis, M.**, **Driver, J.**, **Saade-Castillo, A.**, **Thompson, A. and Koo, J.H.** (2018). Multi-functional ULTEM™ 1010 composite filaments for additive manufacturing using Fused Filament Fabrication (FFF), *Additive Manufacturing*, *24*, 298–306.

[8] **Cicala, G.**, **Ognibene, G.**, **Portuesi, S.**, **Blanco, I.**, **Rapisarda, M.**, **Pergolizzi, E. and Recca, G.** (2018). Comparison of Ultem 9085 used in fused deposition modelling (FDM) with polytherimide blends, *Materials*, *11*(2), 285.

[9] **Yıldız, A.**, **Emanetoğlu, U.**, **Yenigun, E.O. and Cebeci, H.** (2022). Towards optimized carbon nanotubes (CNTs) reinforced polyetherimide (PEI) 3D printed structures: A comparative study on testing standards, *Composite Structures*, *296*, 115853.

[10] **Tatlıdilli, A.**, **Çetin Altındal, D. and Gümüşderelioğlu, M.** (2021). Effects of carbon fiber type and resin ratio on thermal and mechanical lifetime of polyetherimide composites, *Polymer Composites*, *42*(6), 2920–2932.

[11] **Guo, J.**, **Tsou, C.H.**, **Yu, Y.**, **Wu, C.S.**, **Zhang, X.**, **Chen, Z.**, **Yang, T.**, **Ge, F.**, **Liu, P. and Guzman, M.R.D.** (2021). Conductivity and mechanical properties of carbon black-reinforced poly (lactic acid)(PLA/CB) composites, *Iranian Polymer Journal*, *30*(12), 1251–1262.

[12] **Zhang, Y.Y.**, **Sun, Z.**, **Li, Y.Q.**, **Huang, P.**, **Chen, Q. and Fu, S.Y.** (2021). Tensile creep behavior of short-carbon-fiber reinforced polyetherimide composites, *Composites Part B: Engineering*, *212*, 108717.

[13] **Panin, S.**, **Bogdanov, A.**, **Eremin, A.**, **Buslovich, D. and Burkov, M.** (2023). Creep Behavior of Particulate Polyimide and Polyetherimide Based Composites Under Fatigue, *Russian Physics Journal*, *66*(3), 372–377.

[14] **Karabal, M. and Yildiz, A.** (2023). Creep Modeling of 3D Printed Carbon Black Reinforced Polyetherimide Composites, *2023 10th International Conference on Recent Advances in Air and Space Technologies (RAST)*, IEEE, pp.1–6.

[15] **Xu, Y.**, **Wu, Q.**, **Lei, Y. and Yao, F.** (2010). Creep behavior of bagasse fiber reinforced polymer composites, *Bioresource technology*, *101*(9), 3280–3286.

[16] **Jabbar, A.**, **Militkỳ, J.**, **Kale, B.M.**, **Rwawiire, S.**, **Nawab, Y. and Baheti, V.** (2016). Modeling and analysis of the creep behavior of jute/green epoxy composites incorporated with chemically treated pulverized nano/micro jute fibers, *Industrial Crops and Products*, *84*, 230–240.

[17] **Wu, Q.**, **Ogasawara, T.**, **Yoshikawa, N. and Zhai, H.** (2018). Modeling the viscoelasticity of polyetherimide, *Journal of Applied Polymer Science*, *135*(15), 46102.

[18] **Astm, I.** (2015). ASTM52900-15 standard terminology for additive manufacturing—general principles—terminology, *ASTM International, West Conshohocken, PA*, *3*(4), 5.

[19] **Campbell, I.**, **Bourell, D. and Gibson, I.** (2012). Additive manufacturing: rapid prototyping comes of age, *Rapid prototyping journal*, *18*(4), 255–258.

[20] **Jiménez, M.**, **Romero, L.**, **Domínguez, I.A.**, **Espinosa, M.d.M.**, **Domínguez, M.** *et al.* (2019). Additive manufacturing technologies: an overview about 3D printing methods and future prospects, *Complexity*, *2019*.

[21] **Alammar, A.**, **Kois, J.C.**, **Revilla-León, M. and Att, W.** (2022). Additive manufacturing technologies: current status and future perspectives, *Journal of Prosthodontics*, *31*(S1), 4–12.

[22] **Thomas, D.S.**, **Gilbert, S.W.** *et al.* (2014). Costs and cost effectiveness of additive manufacturing, *NIST special publication*, *1176*, 12.

[23] **Mecheter, A.**, **Tarlochan, F. and Kucukvar, M.** (2023). A review of conventional versus additive manufacturing for metals: life-cycle environmental and economic analysis, *Sustainability*, *15*(16), 12299.

[24] **Van Sice, C. and Faludi, J.** (2021). Comparing environmental impacts of metal additive manufacturing to conventional manufacturing, *Proceedings of the Design Society*, *1*, 671–680.

[25] **Blakey-Milner, B.**, **Gradl, P.**, **Snedden, G.**, **Brooks, M.**, **Pitot, J.**, **Lopez, E.**, **Leary, M.**, **Berto, F. and Du Plessis, A.** (2021). Metal additive manufacturing in aerospace: A review, *Materials & Design*, *209*, 110008.

[26] **Zhao, N.**, **Parthasarathy, M.**, **Patil, S.**, **Coates, D.**, **Myers, K.**, **Zhu, H. and Li, W.** (2023). Direct additive manufacturing of metal parts for automotive applications, *Journal of Manufacturing Systems*, *68*, 368–375.

[27] **Lakkala, P.**, **Munnangi, S.R.**, **Bandari, S. and Repka, M.** (2023). Additive manufacturing technologies with emphasis on stereolithography 3D printing in pharmaceutical and medical applications: A review, *International journal of pharmaceutics: X*, *5*, 100159.

[28] **Pal, A.K.**, **Mohanty, A.K. and Misra, M.** (2021). Additive manufacturing technology of polymeric materials for customized products: recent developments and future prospective, *RSC advances*, *11*(58), 36398–36438.

[29] **Praveena, B.**, **Lokesh, N.**, **Buradi, A.**, **Santhosh, N.**, **Praveena, B. and Vignesh, R.** (2022). A comprehensive review of emerging additive manufacturing (3D printing technology): Methods, materials, applications, challenges, trends and future potential, *Materials Today: Proceedings*, *52*, 1309–1313.

[30] **Prashar, G.**, **Vasudev, H. and Bhuddhi, D.** (2023). Additive manufacturing: expanding 3D printing horizon in industry 4.0, *International Journal on Interactive Design and Manufacturing (IJIDeM)*, *17*(5), 2221–2235.

[31] **MarketsandMarkets** (2024). *3D Printing Market by Offering (Service, Printer (Desktop, Industrial), Material (Polymer, Metal, Ceramic), Software), Process (Material Extrusion, VAT Photopolymerization, PBF, Direct Energy Deposition), Application, Vertical, and Region - Global Forecast to 2025*, https://www.marketsandmarkets.com/requestsampleNew.asp?id=1276.

[32] **Dave, H.K. and Patel, S.T.** (2021). Introduction to fused deposition modeling based 3D printing process, *Fused deposition modeling based 3D printing*, 1–21.

[33] **Kaynan, O.**, **Yildiz, A.**, **Bozkurt, Y.E.**, **Ozden Yenigun, E. and Cebeci, H.** (2019). Development of multifunctional CNTs reinforced PEI filaments for fused deposition modeling, *AIAA Scitech 2019 Forum*, p.0406.

[34] **Amancio, S.** (2007). Friction riveting. Development and analysis of a new joining technique for polymer-metal multi-materials structures.

[35] **Gardiner, G.** (2006). Thermoplastic composites gain leading edge on the A380: breakthrough manufacturing process produces lightweight, affordable glass-reinforced PPS J-nose on the worlds largest commercial aircraft wing, *High Performance Composites*, *14*(2), 50.

[36] **McCrum, N.G.**, **Buckley, C.P. and Bucknall, C.B.** (1997). *Principles of polymer engineering*, Oxford University Press.

[37] **Osswald, T. and Menges, G.** (2012). Part 3: Engineering design properties: Mechanical behavior of polymers, *Mater. Sci. Polym. Eng*, *339*, 341–422.

[38] **Boltzmann, L.** (1878). Zur theorie der elastischen nachwirkung, *Annalen der Physik*, *241*(11), 430–432.

[39] **Yang, J.L.**, **Zhang, Z.**, **Schlarb, A.K. and Friedrich, K.** (2006). On the characterization of tensile creep resistance of polyamide 66 nanocomposites. Part II: Modeling and prediction of long-term performance, *Polymer*, *47*(19), 6745–6758.

[40] **Huang, C.**, **Gao, D.**, **Meng, T. and Yang, C.** (2023). Investigation into viscoelastic properties of fiber-reinforced asphalt composite concrete based on the burgers model, *Buildings*, *13*(2), 449.

[41] **Dey, A. and Basudhar, P.** (2010). Applicability of Burger model in predicting the response of viscoelastic soil beds, *GeoFlorida 2010: Advances in Analysis, Modeling & Design*, 2611–2620.

[42] **Acha, B.A.**, **Reboredo, M.M. and Marcovich, N.E.** (2007). Creep and dynamic mechanical behavior of PP–jute composites: Effect of the interfacial adhesion, *Composites Part A: Applied Science and Manufacturing*, *38*(6), 1507–1516.

[43] **Hajikarimi, P. and Nejad, F.M.** (2021). *Applications of viscoelasticity: Bituminous materials characterization and modeling*, Elsevier.

[44] **Ward, I.M. and Sweeney, J.** (2012). *Mechanical properties of solid polymers*, John Wiley & Sons.

[45] **Finley, W.N.**, **Lai, J.S. and Onaran, K.** (1976). Creep and Relaxation of Nonlinear Viscoelastic Material.

[46] **Perez, C.J.**, **Alvarez, V.A. and Vazquez, A.** (2008). Creep behaviour of layered silicate/starch–polycaprolactone blends nanocomposites, *Materials Science and Engineering: A*, *480*(1-2), 259–265.

[47] **Sá, M.F., Gomes, A.M., Correia, J.R. and Silvestre, N.** (2011). Creep behavior of pultruded GFRP elements–Part 2: Analytical study, *Composite structures*, *93*(9), 2409–2418.

[48] **Tajvidi, M., Falk, R.H. and Hermanson, J.C.** (2005). Time–temperature superposition principle applied to a kenaf-fiber/high-density polyethylene composite, *Journal of applied polymer science*, *97*(5), 1995–2004.

[49] **Plota, A. and Masek, A.** (2020). Lifetime prediction methods for degradable polymeric materials—A short review, *Materials*, *13*(20), 4507.

[50] **Williams, M.L., Landel, R.F. and Ferry, J.D.** (1955). The temperature dependence of relaxation mechanisms in amorphous polymers and other glass-forming liquids, *Journal of the American Chemical society*, *77*(14), 3701–3707.

[51] **Meneses, A., Naya, S., Francisco-Fernández, M., López-Beceiro, J., Gracia-Fernández, C. and Tarrío-Saavedra, J.** (2023). TTS package: Computational tools for the application of the Time Temperature Superposition principle, *Heliyon*, *9*(5).

[52] **Naya, S., Meneses, A., Tarrío-Saavedra, J., Artiaga, R., López-Beceiro, J. and Gracia-Fernández, C.** (2013). New method for estimating shift factors in time–temperature superposition models, *Journal of thermal analysis and calorimetry*, *113*, 453–460.

[53] (2020). *D3822/D3822M 14 (Reapproved 2020) Standard Test Method for Tensile Properties of Single Textile Fibers*, `https://doi.org/10.1520/D3822_D3822M-14R20`.

[54] **Amancio-Filho, S., Roeder, J., Nunes, S., Dos Santos, J. and Beckmann, F.** (2008). Thermal degradation of polyetherimide joined by friction riveting (FricRiveting). Part I: Influence of rotation speed, *Polymer degradation and stability*, *93*(8), 1529–1538.

[55] **Kuroda, S.i., Terauchi, K., Nogami, K. and Mita, I.** (1989). Degradation of aromatic polymers—I. Rates of crosslinking and chain scission during thermal degradation of several soluble aromatic polymers, *European polymer journal*, *25*(1), 1–7.

[56] **Augh, L., Gillespie Jr, J. and Fink, B.** (2001). Degradation of continuous carbon fiber reinforced polyetherimide composites during induction heating, *Journal of Thermoplastic Composite Materials*, *14*(2), 96–115.

[57] **Rinaldi, M., Ghidini, T. and Nanni, F.** (2021). Fused filament fabrication of polyetheretherketone/multiwalled carbon nanotube nanocomposites: The effect of thermally conductive nanometric filler on the printability and related properties, *Polymer International*, *70*(8), 1080–1089.

[58] **Kalaitzidou, K.**, **Fukushima, H. and Drzal, L.T.** (2007). Multifunctional polypropylene composites produced by incorporation of exfoliated graphite nanoplatelets, *Carbon*, *45*(7), 1446–1452.

[59] **Gao, X.**, **Isayev, A.I. and Yi, C.** (2016). Ultrasonic treatment of polycarbonate/carbon nanotubes composites, *Polymer*, *84*, 209–222.

[60] **Kharchenko, S.B.**, **Douglas, J.F.**, **Obrzut, J.**, **Grulke, E.A. and Migler, K.B.** (2004). Flow-induced properties of nanotube-filled polymer materials, *Nature materials*, *3*(8), 564–568.

[61] **Verma, P.**, **Verma, M.**, **Gupta, A.**, **Chauhan, S.S.**, **Malik, R.S. and Choudhary, V.** (2016). Multi walled carbon nanotubes induced viscoelastic response of polypropylene copolymer nanocomposites: Effect of filler loading on rheological percolation, *Polymer Testing*, *55*, 1–9.

[62] **Du, F.**, **Scogna, R.C.**, **Zhou, W.**, **Brand, S.**, **Fischer, J.E. and Winey, K.I.** (2004). Nanotube networks in polymer nanocomposites: rheology and electrical conductivity, *Macromolecules*, *37*(24), 9048–9055.

[63] **Ajinjeru, C.**, **Kishore, V.**, **Lindahl, J.**, **Sudbury, Z.**, **Hassen, A.A.**, **Post, B.**, **Love, L.**, **Kunc, V. and Duty, C.** (2018). The influence of dynamic rheological properties on carbon fiber-reinforced polyetherimide for large-scale extrusion-based additive manufacturing, *The International Journal of Advanced Manufacturing Technology*, *99*, 411–418.

[64] **Bangarusampath, D.**, **Ruckdäschel, H.**, **Altstädt, V.**, **Sandler, J.K.**, **Garray, D. and Shaffer, M.S.** (2009). Rheology and properties of melt-processed poly (ether ether ketone)/multi-wall carbon nanotube composites, *Polymer*, *50*(24), 5803–5811.

[65] **Pötschke, P.**, **Fornes, T. and Paul, D.** (2002). Rheological behavior of multiwalled carbon nanotube/polycarbonate composites, *Polymer*, *43*(11), 3247–3255.

[66] **Kausar, A. and Taherian, R.** (2019). Electrical conductivity behavior of polymer nanocomposite with carbon nanofillers, *Electrical Conductivity in Polymer-Based Composites: Experiments, Modelling and Applications*, 41–72.

[67] *ULTEM™ Resin 1010 Global Technical Data Sheet*, https://www.sabic.com/en/search/product-documents?q=ULTEM%20Resin, accessed: 2024-07-02.

[68] **Pitchan, M.K.**, **Bhowmik, S.**, **Balachandran, M. and Abraham, M.** (2016). Effect of surface functionalization on mechanical properties and decomposition kinetics of high performance polyetherimide/MWCNT nano composites, *Composites Part A: Applied Science and Manufacturing*, *90*, 147–160.

[69] **Dul, S., Fambri, L. and Pegoretti, A.** (2018). Filaments production and fused deposition modelling of ABS/carbon nanotubes composites, *Nanomaterials*, *8*(1), 49.

[70] **Zhao, J., Dai, K., Liu, C., Zheng, G., Wang, B., Liu, C., Chen, J. and Shen, C.** (2013). A comparison between strain sensing behaviors of carbon black/polypropylene and carbon nanotubes/polypropylene electrically conductive composites, *Composites Part A: Applied Science and Manufacturing*, *48*, 129–136.

[71] **Ghosh, S.K., Rajesh, P., Srikavya, B., Rathore, D.K., Prusty, R.K. and Ray, B.C.** (2018). Creep behaviour prediction of multi-layer graphene embedded glass fiber/epoxy composites using time-temperature superposition principle, *Composites Part A: Applied Science and Manufacturing*, *107*, 507–518.

[72] **Isayev, A., Kumar, R. and Lewis, T.M.** (2009). Ultrasound assisted twin screw extrusion of polymer–nanocomposites containing carbon nanotubes, *Polymer*, *50*(1), 250–260.

[73] **Zhang, Y.Y., Mo, X.L., Guan, B.W., Chen, Q., Huang, P., Li, Y.Q. and Fu, S.Y.** (2022). Experimental and theoretical investigations of the viscoelastic behaviour of short carbon fiber reinforced polyetherimide composites, *Composite Structures*, *298*, 116016.

[74] **Panin, S.V., Bogdanov, A.A., Eremin, A.V., Buslovich, D.G. and Shilko, I.S.** (2023). Effect of Polymer Matrix on Inelastic Strain Development in PI-and PEI-Based Composites Reinforced with Short Carbon Fibers under Low-Cyclic Fatigue, *Polymers*, *15*(5), 1228.

[75] **Alghamdi, A.S., Ashcroft, I.A. and Song, M.** (2014). Creep resistance of novel polyethylene/carbon black nanocomposites, *Int J Mater Sci Eng*, *15*, 16.

[76] **Mostafa, A., Abouel-Kasem, A., Bayoumi, M. and El-Sebaie, M.** (2009). On the influence of CB loading on the creep and relaxation behavior of SBR and NBR rubber vulcanizates, *Materials & Design*, *30*(7), 2721–2725.

[77] **Abdulla, F.A., Fadhil, H.A. and Abdulwahid, J.N.** (2018). Experimental Study of the Creep Behaviour of Nano-Composites Carbon Fibres, *IOP Conference Series: Materials Science and Engineering*, volume454, IOP Publishing, p.012126.

[78] **Liu, X., Pan, Y., Zheng, G. and Schubert, D.W.** (2016). Rheological and electrical behavior of poly (methyl methacrylate)/carbon black composites as investigated by creep recovery in shear, *Composites Science and Technology*, *128*, 1–7.

[79] **Tofangchi, A., Han, P., Izquierdo, J., Iyengar, A. and Hsu, K.** (2019). Effect of ultrasonic vibration on interlayer adhesion in fused filament fabrication 3D printed ABS, *Polymers*, *11*(2), 315.

[80] **Stano, G.**, **Pavone, A.**, **Jafor, M.A.**, **Matalgah, K.**, **Percoco, G. and Fleck, T.J.** (2024). Enhancing the sensitivity of 3D printed sensors via ironing and void reduction, *Virtual and Physical Prototyping*, *19*(1), e2331153.

[81] **Stano, G.**, **Sayah, N.**, **Smith, D.E. and Fleck, T.J.** (2024). Effect of Process Parameters in Additively Manufactured Sensors prepared via Material Extrusion Processes: Correlation among Electrical, Mechanical and Microstructure Properties, *Additive Manufacturing Letters*, *9*, 100194.

APPENDICES

APPENDIX A : Creep Modeling Parameters' Tables

APPENDIX A : Creep Modeling Parameters' Tables

Table A.1 : Parameter values were obtained by fitting the Burgers model with reduced χ^2 and adjusted R^2 values for specimens tested under a double cantilever fixture.

Sample	Temp. (°C)	E_M (MPa)	E_K (MPa)	η_M (MPa.s)	η_K (MPa.s)	Red. χ^2	Adj. R^2
Neat PEI	30	1.47E+03	2.47E+04	2.68E+07	2.20E+06	4.16E-07	0.990
	50	1.37E+03	2.67E+04	3.13E+07	2.24E+06	4.54E-07	0.986
	70	1.31E+03	2.87E+04	3.35E+07	2.25E+06	4.47E-07	0.984
	90	1.25E+03	3.24E+04	3.57E+07	2.79E+06	4.09E-07	0.983
	110	1.19E+03	3.54E+04	3.43E+07	3.27E+06	3.18E-07	0.987
	130	1.14E+03	3.29E+04	3.01E+07	3.67E+06	2.97E-07	0.991
	150	1.08E+03	2.43E+04	1.79E+07	3.03E+06	3.57E-07	0.996
	170	9.80E+02	1.20E+04	6.79E+06	1.63E+06	8.62E-07	0.998
5 wt% CB/PEI	30	2.34E+03	4.32E+04	4.02E+07	3.05E+06	1.51E-07	0.990
	50	2.24E+03	3.51E+04	3.90E+07	3.34E+06	2.28E-07	0.989
	70	2.16E+03	3.69E+04	4.21E+07	3.45E+06	2.54E-07	0.987
	90	2.12E+03	4.03E+04	4.22E+07	3.78E+06	2.20E-07	0.987
	110	2.09E+03	4.20E+04	3.85E+07	4.49E+06	2.00E-07	0.990
	130	2.03E+03	3.60E+04	2.94E+07	4.52E+06	1.88E-07	0.994
	150	1.92E+03	2.36E+04	1.57E+07	3.32E+06	2.67E-07	0.997
	170	1.63E+03	1.17E+04	6.24E+06	1.79E+06	6.52E-07	0.999
10 wt% CB/PEI	30	2.39E+03	3.59E+04	3.65E+07	3.98E+06	1.74E-07	0.993
	50	2.27E+03	4.43E+04	4.93E+07	4.24E+06	1.45E-07	0.989
	70	2.25E+03	4.76E+04	5.05E+07	4.37E+06	1.49E-07	0.988
	90	2.23E+03	5.26E+04	5.12E+07	5.16E+06	1.43E-07	0.987
	110	2.19E+03	5.36E+04	5.30E+07	6.50E+06	1.22E-07	0.990
	130	2.15E+03	5.11E+04	4.41E+07	6.21E+06	9.56E-08	0.994
	150	2.08E+03	4.14E+04	3.40E+07	5.56E+06	1.10E-07	0.996
	170	1.94E+03	2.69E+04	1.67E+07	3.78E+06	1.92E-07	0.998

Table A.2 : Parameter values were obtained by fitting the Findley model with Red. χ^2 and Adj. R^2 values for specimens tested under a double cantilever fixture.

Sample	Temperature °C	ε_0	A	n	Red. χ^2	Adj. R^2
Neat PEI	30	2.52e–01	1.38e–02	1.86e–01	3.02e–08	0.999
	50	2.66e–01	1.88e–02	1.47e–01	4.15e–08	0.999
	70	2.80e–01	1.99e–02	1.35e–01	5.27e–08	0.998
	90	3.01e–01	1.39e–02	1.60e–01	7.04e–08	0.997
	110	3.23e–01	7.81e–03	2.14e–01	7.08e–08	0.997
	130	3.41e–01	5.26e–03	2.71e–01	6.67e–08	0.998
	150	3.63e–01	3.65e–03	3.67e–01	6.99e–08	0.999
	170	3.98e–01	3.99e–03	4.67e–01	1.07e–07	0.999
5 wt% CB/PEI	30	1.61e–01	6.84e–03	2.04e–01	2.92e–08	0.998
	50	1.64e–01	9.62e–03	1.87e–01	2.28e–08	0.999
	70	1.69e–01	1.08e–02	1.71e–01	3.17e–08	0.998
	90	1.77e–01	7.94e–03	1.95e–01	3.60e–08	0.998
	110	1.84e–01	4.49e–03	2.61e–01	4.28e–08	0.998
	130	1.90e–01	3.02e–03	3.35e–01	4.05e–08	0.999
	150	2.01e–01	2.56e–03	4.24e–01	4.49e–08	0.999
	170	2.36e–01	3.16e–03	5.09e–01	6.27e–08	1.000
10 wt% CB/PEI	30	1.58e–01	5.57e–03	2.49e–01	1.89e–08	0.999
	50	1.65e–01	7.59e–03	1.88e–01	1.57e–08	0.999
	70	1.67e–01	6.98e–03	1.91e–01	2.05e–08	0.998
	90	1.72e–01	4.84e–03	2.23e–01	2.82e–08	0.998
	110	1.76e–01	3.39e–03	2.63e–01	3.01e–08	0.997
	130	1.81e–01	2.50e–03	3.11e–01	2.14e–08	0.999
	150	1.87e–01	2.29e–03	3.52e–01	2.29e–08	0.999
	170	2.01e–01	1.99e–03	4.45e–01	2.96e–08	0.999

Table A.3 : Parameter values were obtained by fitting the Burgers model with reduced χ^2 and adjusted R^2 values for specimens tested under a three-point bending fixture.

Sample	Temp. (°C)	E_M (MPa)	E_K (MPa)	η_M (MPa.s)	η_K (MPa.s)	Red. χ^2	Adj. R^2
Neat PEI	30	2338	48242	3.86E+07	2.32E+06	7.03E-08	0.986
	50	2253	36158	3.38E+07	3.23E+06	1.05E-07	0.990
	70	2176	39382	3.64E+07	3.16E+06	8.38E-08	0.990
	90	2101	44044	4.88E+07	3.63E+06	5.74E-08	0.990
	110	2051	51083	5.82E+07	4.12E+06	3.91E-08	0.991
	130	2018	53071	4.76E+07	4.12E+06	3.03E-08	0.994
	150	1963	40965	2.19E+07	3.07E+06	3.36E-08	0.998
	170	1751	17796	5.69E+06	1.48E+06	1.16E-07	0.999
	190	1153	4976	1.18E+06	4.60E+05	1.57E-06	1.000
5 wt% CB/PEI	30	2717	60966	4.39E+07	3.54E+06	5.09E-08	0.987
	50	2619	37309	5.09E+07	3.98E+06	5.82E-08	0.993
	70	2563	41505	5.21E+07	3.70E+06	4.30E-08	0.993
	90	2509	46184	6.31E+07	3.98E+06	2.99E-08	0.994
	110	2472	53095	6.88E+07	4.45E+06	2.15E-08	0.994
	130	2452	58860	5.74E+07	4.58E+06	1.78E-08	0.995
	150	2413	49361	3.11E+07	3.52E+06	1.65E-08	0.998
	170	2216	25144	8.76E+06	1.98E+06	4.37E-08	0.999
	190	1549	6218	1.75E+06	6.64E+05	8.73E-07	0.999
10 wt% CB/PEI	30	2491	59939	5.31E+07	2.59E+06	4.68E-08	0.983
	50	2427	35591	4.29E+07	3.35E+06	6.59E-08	0.993
	70	2368	39114	4.48E+07	3.13E+06	4.97E-08	0.993
	90	2309	44162	5.50E+07	3.42E+06	3.51E-08	0.993
	110	2270	50724	6.46E+07	3.89E+06	2.57E-08	0.993
	130	2245	54508	5.85E+07	4.03E+06	2.18E-08	0.994
	150	2200	48023	3.23E+07	3.05E+06	1.95E-08	0.997
	170	2024	24503	7.87E+06	1.78E+06	5.90E-08	0.999
	190	1419	6234	1.81E+06	6.36E+05	9.25E-07	0.999
HP-Neat PEI	30	2789	66357	4.68E+07	3.12E+06	4.07E-08	0.987
	50	2688	44155	4.47E+07	4.51E+06	5.57E-08	0.992
	70	2621	47045	4.81E+07	4.13E+06	4.55E-08	0.992
	90	2576	49400	6.48E+07	4.39E+06	3.24E-08	0.993
	110	2551	52909	6.83E+07	4.61E+06	1.84E-08	0.995
	130	2522	53140	5.94E+07	4.53E+06	1.34E-08	0.997
	150	2473	47481	3.38E+07	3.82E+06	1.27E-08	0.998
	170	2337	30121	1.23E+07	2.38E+06	2.09E-08	0.999
	190	1839	7617	2.05E+06	7.95E+05	6.22E-07	0.999

Table A.4 : Parameter values were obtained by fitting the Findley model with Red. χ^2 and Adj. R^2 values for specimens tested under a three-point bending fixture.

Sample	Temp. °C	ε_0	A	n	Red. χ^2	Adj. R^2
Neat PEI	30	0.1155	0.0108	0.1209	5.62E-09	0.999
	50	0.1242	0.0060	0.2079	2.75E-08	0.997
	70	0.1283	0.0068	0.1850	1.92E-08	0.998
	90	0.1325	0.0077	0.1555	2.17E-08	0.996
	110	0.1369	0.0072	0.1472	1.74E-08	0.996
	130	0.1423	0.0046	0.1946	1.31E-07	0.976
	150	0.1489	0.0023	0.3331	7.30E-09	0.999
	170	0.1672	0.0020	0.5060	2.42E-08	1.000
	190	0.2502	0.0046	0.6054	2.98E-07	1.000
5 wt% CB/PEI	30	0.1038	0.0050	0.1772	6.40E-09	0.998
	50	0.1061	0.0056	0.1994	3.99E-08	0.995
	70	0.1071	0.0073	0.1627	2.94E-08	0.995
	90	0.1092	0.0080	0.1426	2.94E-08	0.994
	110	0.1126	0.0067	0.1458	2.12E-08	0.994
	130	0.1163	0.0044	0.1838	1.02E-08	0.997
	150	0.1202	0.0026	0.2797	7.53E-09	0.999
	170	0.1322	0.0017	0.4745	1.88E-08	1.000
	190	0.1840	0.0039	0.5822	3.61E-08	1.000
10 wt% CB/PEI	30	0.1032	0.0156	0.0764	3.41E-09	0.999
	50	0.1135	0.0071	0.1828	3.61E-08	0.996
	70	0.1149	0.0090	0.1505	2.62E-08	0.996
	90	0.1175	0.0099	0.1288	2.64E-08	0.995
	110	0.1210	0.0090	0.1243	2.15E-08	0.995
	130	0.1252	0.0065	0.1502	1.36E-08	0.996
	150	0.1312	0.0036	0.2395	9.33E-09	0.999
	170	0.1453	0.0016	0.4886	3.34E-08	1.000
	190	0.2012	0.0042	0.5648	3.84E-08	1.000
HP-Neat PEI	30	0.1008	0.0055	0.1564	6.05E-09	0.998
	50	0.1055	0.0038	0.2346	2.23E-08	0.997
	70	0.1070	0.0052	0.1914	1.67E-08	0.997
	90	0.1075	0.0067	0.1540	2.34E-08	0.995
	110	0.1099	0.0058	0.1606	2.26E-08	0.994
	130	0.1125	0.0046	0.1867	1.96E-08	0.995
	150	0.1170	0.0027	0.2762	1.19E-08	0.998
	170	0.1251	0.0018	0.4299	1.87E-08	0.999
	190	0.1555	0.0031	0.5893	3.41E-08	1.000

Table A.5 : Parameter values were obtained by fitting the generalized Kelvin-Voigt Model with Red. χ^2 and Adj. R^2 values for specimens tested under a three-point bending fixture.

Sample	Temp. (°C)	E_1	E_2	E_3	N_2	N_3	Red. χ^2	Adj. R^2
Neat PEI	30	2381.506	52910.46	38003.38	586439.9	9893489	2.09E-08	0.996
	50	2322.104	49964.77	24788.11	359940.7	5791236	1.58E-08	0.999
	70	2232.794	53275.18	27833.9	390948.2	6233933	2.02E-08	0.998
	90	2155.033	58435.91	33353.21	306443.4	6493005	1.75E-08	0.997
	110	2094.815	68521.17	39267.99	334611.2	7.35E+06	1.56E-08	0.996
	130	2033.892	93911.76	38308.66	1579958	9559410	1.80E-08	0.996
	150	1970.557	61003.93	18699.71	2313200	9.76E+06	2.24E-08	0.998
	170	1764.049	4135.419	27660.1	3304930	1131424	5.10E-08	1.000
	190	1180.651	796.4854	8672.31	722537.7	310313.6	2.64E-07	1.000
5 wt% CB/PEI	30	2772.053	41423.44	68150.38	1.11E+07	6.67E+05	1.11E-08	0.997
	50	2698.773	64743.41	28327.57	372977.2	5785231	8.50E-09	0.999
	70	2626.662	70250.15	32264.52	443710.8	6105283	1.47E-08	0.998
	90	2567.536	77194.01	37029.2	383276.1	6.40E+06	1.48E-08	0.997
	110	2512.113	97767.68	42420.12	637507.9	7.53E+06	1.37E-08	0.996
	130	2462.555	100000	46856.68	3176401	1.36E+07	1.11E-08	0.997
	150	2417.912	64535.13	25244.27	3095818	1.58E+07	1.29E-08	0.998
	170	2225.068	34508.07	5753.909	1728127	5599360	2.74E-08	1.000
	190	1589.261	1266.799	12842.13	945191.5	440029	1.25E-07	1.000
10 wt% CB/PEI	30	2531.355	52672.02	62889.24	1.28E+07	652340.5	1.50E-08	0.995
	50	2492.794	60531.27	26890.68	423954.4	5459095	1.41E-08	0.998
	70	2414.814	67468.24	30790.55	614887.9	6024332	2.27E-08	0.997
	90	2349.164	77298.57	36072.14	613838.8	6.46E+06	2.25E-08	0.996
	110	2284.299	99563.61	45067.52	2134232	9.38E+06	1.77E-08	0.996
	130	2255.009	93223.69	47000.86	2735078	1.23E+07	1.35E-08	0.997
	150	2203.481	58194.81	25595.9	2694030	1.78E+07	1.64E-08	0.998
	170	2033.411	33137.51	5207.871	1466271	5101744	3.35E-08	1.000
	190	1453.279	1339.376	12262.31	972928.4	418290.9	1.45E-07	1.000
HP-Neat PEI	30	2835.292	47303.6	70303.37	1.37E+07	759754.7	1.25E-08	0.99
	50	2767.797	29997.13	66607.55	6992014	401743.2	8.41E-09	0.999
	70	2685.044	33835.3	71130.43	7241023	482112.6	1.24E-08	0.998
	90	2637.096	78752.92	38810.4	400388.9	7058592	1.19E-08	0.997
	110	2593.606	100000	41512.93	592054.7	7.45E+06	1.32E-08	0.997
	130	2529.036	46052.71	93354.23	1.38E+07	4045706	9.86E-09	0.998
	150	2477.614	66923.99	27829.8	3504582	1.50E+07	9.07E-09	0.999
	170	2340.653	36461.04	6505.052	2273569	8869402	1.74E-08	1.000
	190	1887.109	1473.821	15293.21	1135450	514158.4	9.12E-08	1.000

CURRICULUM VITAE

Name SURNAME: Merve KARABAL

EDUCATION:

- **B.Sc.:** 2022, Istanbul Technical University, Faculty of Aeronautical and Astronautical Engineering, Aeronautical and Astronautical Engineering Department
- **M.Sc.:** 2024, Istanbul Technical University, Faculty of Aeronautical and Astronautical Engineering, Aeronautical and Astronautical Engineering Programme

PROFESSIONAL EXPERIENCE AND REWARDS:

- ITU Aerospace Research Center (ITU ARC)-Nanomaterials, Textiles and Advanced Composites Research Group

  Researcher, March 2021 – Today

PUBLICATIONS, PRESENTATIONS AND PATENTS ON THE THESIS:

- Kayginok, F., **Karabal, M.**, Yildiz, A., Emanetoglu, U., Cebeci, H. (2022). Evaluation of Creep Behavior of 3D Printed CB/PEI Composites. *Additive Manufacturing Conference Türkiye 2022 (AMCTURKEY 2022)*, October 6-8, 2022 Kusadasi, Aydin. (Presentation)
- **Karabal M.**, Yildiz A. (2023). Creep Modeling of 3D Printed Carbon Black Reinforced Polyetherimide Composites. *10th International Conference on Recent Advances in Air and Space Technologies (RAST)*, June 7-9, 2023 Istanbul, Turkey. (Presentation)
- **Karabal M.**, Yildiz A. (2024). Creep Resistance Enhancement and Modeling of 3D Printed Polyetherimide/Carbon Black Composites, *Composite Structures,* under revision. (Article)

OTHER PUBLICATIONS, PRESENTATIONS AND PATENTS:

- Kayginok, F., **Karabal, M.**, Yıldız, A., Yidiz, K., Cebeci, H. (2023). Establishing the Polymer Effect on the Viscoelastic Properties of CNTs Reinforced PEI and PEEK *25th International Conference on Composite of Structures (ICCS25)*, July 19 - 22, 2022 Porto, Portugal. (Presentation)

- **Karabal M.**, Yuksel R., Kayginok F., Yildiz A., Cebeci H (2023). Embedded Piezoresistive Sensors Printed by FFF for Aerospace Applications. *AIAA SCITECH 2023 Forum*, January 23-27, 2023 National Harbor, Maryland, USA. (Presentation)

- **Karabal M.**, Dincer M., Arslan D., Yuksel R., Akyazici Z.N., Yildiz A., Cebeci H (2023). Direct 3D Printing of Strain Sensors onto 3D Woven Orthogonal Composite Structures: Evaluating Two Distinct Approaches for Sensor Performance. *AIAA SCITECH 2024 Forum*, January 8-12, 2024 Orlando, Florida, USA. (Presentation)

- Kayginok F., **Karabal M.**, Yildiz A., Cebeci H (2024). CNT Reinforced PEI and PEEK nanocomposites: A Comparison on the Thermal and Rheological Properties, *Polymer Testing* under revision. (Article)